Causes of the Multidecadal-Scale Warming of the Intermediate Water in the Okhotsk Sea and Western Subarctic North Pacific

TAKUYA NAKANOWATARI AND TOMOHIRO NAKAMURA

Institute of Low Temperature Science, Hokkaido University, Sapporo, Japan

KEISUKE UCHIMOTO

Research Institute of Innovative Technology for the Earth, Kyoto, Japan

HIROKI UEHARA, HUMIO MITSUDERA, AND KAY I. OHSHIMA

Institute of Low Temperature Science, Hokkaido University, Sapporo, Japan

HIROYASU HASUMI

Atmosphere and Ocean Research Institute, University of Tokyo, Chiba, Japan

MASAAKI WAKATSUCHI

Institute of Low Temperature Science, Hokkaido University, Sapporo, Japan

(Manuscript received 28 February 2014, in final form 18 August 2014)

ABSTRACT

Causes of the multidecadal-scale warming of the intermediate water in the Okhotsk Sea and the western subarctic North Pacific during 1980–2008 are investigated using an ice–ocean coupled model with interannually varying atmospheric forcing. A hindcast experiment qualitatively reproduces the warming and decadal fluctuations of the intermediate water that are similar to those of observations: the warming is significant along the western part of the Okhotsk Sea and subarctic frontal region. The effects of the thermohaline- and wind-driven ocean circulation on the warming are evaluated from perturbation experiments on thermohaline (turbulent heat and freshwater fluxes) and wind causes, respectively. The thermohaline causes are shown to contribute positively to warming in the Okhotsk Sea Intermediate Water (OSIW). The heat budget analysis for the OSIW indicates that the warming is related to a decrease in cold and dense shelf water (DSW) flux, which is caused by a decrease in sea ice and surface water freshening. In contrast, the wind cause has a cooling effect in the OSIW through an increase in DSW. In the subarctic frontal region, the warming is mainly caused by the wind stress change. The heat budget analysis indicates that the warming is related to an increase in the northward advection of the subtropical warm water. These results imply that both thermohaline- and wind-driven ocean circulation changes are essential components of the warming in the intermediate water. The atmospheric conditions responsible for the warming are related to a weakened Aleutian low and Siberian high in early and late winter.

1. Introduction

The Okhotsk Sea is a marginal sea located on the northwest rim of the Pacific Ocean, and is known to be the ventilation source of North Pacific Intermediate Water (Talley 1991; Yasuda 1997; Watanabe and Wakatsuchi 1998). A large amount of sea ice within the Okhotsk Sea is produced along the northwestern coastal polynyas by severe wintertime winds blowing from the Eurasian continent (Martin et al. 1998; Ohshima et al. 2003; Nihashi et al. 2009; Kawaguchi et al. 2010), and the brine rejection associated with sea ice production leads to vertical convection of up to 27.0σ_θ [σ_θ is defined as potential density $-$ 1000 (kg m^{-3}); thus, the density of seawater 1027.0 kg m^{-3} means 27.0σ_θ], resulting in the formation of cold, oxygen-rich, dense shelf water (DSW) (Kitani 1973; Gladyshev et al. 2000; Shcherbina et al. 2003;

Corresponding author address: Takuya Nakanowatari, Japan Agency for Marine-Earth Science and Technology, 2-15 Natsushima-cho, Yokosuka, 237-0061, Japan.
E-mail: nakanow@jamstec.go.jp

DOI: 10.1175/JCLI-D-14-00172.1

Nakamura et al. 2006; Matsuda et al. 2009). DSW is transported southward by the cyclonic ocean circulation in the Okhotsk Sea (Mizuta et al. 2003; Fukamachi et al. 2004), and it then mixes with the warm, saline water originating from the North Pacific. The resulting mixed water is called Okhotsk Sea Mode Water (Yasuda 1997) or Okhotsk Sea Intermediate Water (OSIW; Itoh et al. 2003). OSIW is cold, has a low salinity, and is thick relative to the intermediate water in the North Pacific at (26.7–27.0)σ_θ.

The dynamical processes related to the strong tidal currents around the Kuril Straits are also important for the ventilation of the Okhotsk Sea and the formation of OSIW. The effective amplification of topographically trapped waves generated by the subinertial diurnal tides cause considerable intensification of the tidal flow around the Kuril Straits, and this strengthened tidal flow generates internal lee waves with large amplitudes over sills. The breaking of the waves thus leads to enhanced vertical mixing (Nakamura and Awaji 2004), and the topographically trapped waves also induce a strong velocity shear near the sills, which results in bottom-confined intense mixing (Tanaka et al. 2010). The importance of tidal mixing on the formation of the OSIW was indicated by a numerical study (Nakamura et al. 2006) and observational data (Nakamura et al. 2010).

The OSIW outflows from the Okhotsk Sea to the North Pacific through the Kuril Straits (mainly through the Bussol' Strait; Talley 1991; Kawasaki and Kono 1994; Ohshima et al. 2010) and spreads to the subarctic and subtropical gyres after being modified by the Oyashio water and by mixing with the Kuroshio Water (Yasuda 1997). Recent studies have suggested that the water exchange between the Okhotsk Sea and the North Pacific is governed by the strength of the subarctic gyre in the North Pacific (Andreev and Shevchenko 2008; Ohshima et al. 2010). Based on a combination of outputs from the Ocean General Circulation Model for Earth Simulator (Masumoto et al. 2004), and hydrography, Katsumata and Yasuda (2010) have estimated the exchange transport to be ~10 Sv in winter (1 Sv $\equiv$ $10^6\,m^3\,s^{-1}$).

Much attention has been focused on the role that ventilation in the Okhotsk Sea plays in the cycle of chemical properties in the North Pacific (Warner et al. 1996; Wong et al. 1998; Yamamoto-Kawai et al. 2004; Uchimoto et al. 2011). Hansell et al. (2002) indicated that the concentration of dissolved organic carbon (DOC) is higher in the intermediate layer of the Okhotsk Sea than in the intermediate layer of the North Pacific. Mooring observations in the northwestern shelf region of the Okhotsk Sea have revealed that the overturning circulation in relation to sea ice production transports DOC into the intermediate layer of the Okhotsk Sea (Nakatsuka et al. 2004). It has also been shown that the concentration of iron, which is an essential nutrient for phytoplankton and is associated with a rich DOC, is also high in the intermediate layer of the Okhotsk Sea (Nishioka et al. 2007; Uchimoto et al. 2014). Thus, the ventilation in the Okhotsk Sea is thought to play a key role in the dynamics of the marine ecosystem in the subarctic region.

A half-century-scale warming (Hill et al. 2003; Itoh 2007; Nakanowatari et al. 2007) and decadal-scale variability (Osafune and Yasuda 2006) have recently been discovered within the intermediate-water temperature in the Okhotsk Sea. Since the warming signal is significant along the pathway of the DSW, and is accompanied by a decrease in dissolved oxygen, Nakanowatari et al. (2007) suggested that the warming is caused by a reduction in the production of DSW, and further suggested that this decrease is caused by a reduction in sea ice production during winter. Consistent with their suggestion, it is known that the wintertime upwind air temperature has significantly increased during the past 50 yr (Serreze et al. 2000). Recently, Uehara et al. (2014) indicated that the DSW exhibits a significant freshening trend during the past 50 yr from an analysis of a newly complied hydrographic dataset augmented by Russian observations in the Sea of Okhotsk. From the sea ice production estimated from heat flux calculations using satellite-based ice thickness and atmospheric reanalysis data, it was also reported that the sea ice production has decreased by 11% for the past 34 yr (Kashiwase et al. 2014).

Through changes in the DSW, model simulations support the significant effect of air temperature variability over the Okhotsk Sea on the ocean temperature at intermediate depths. Matsuda et al. (2009) showed that a surface air temperature warming of 3°C over the Okhotsk Sea leads to a decrease in DSW, which then results in a warming of the OSIW at 26.8σ_θ by 0.6°C. In addition, Fujisaki et al. (2011) focused on DSW formation processes from 1998 to 2000, and found that the density of DSW is controlled by ice production: the larger ice production leads to the higher DSW density.

However, two other causes for the decrease in DSW have been suggested: surface freshwater flux, and wind-driven circulation. For example, upper ocean freshening due to surface freshwater flux would strengthen the stratification, and thus weaken the ventilation or production of DSW. It is noted that a 50-yr scale decrease in sea surface salinity (SSS) has been observed in the northern North Pacific, and this has been attributed to an enhancement of the global hydrological cycle (Hosoda et al. 2009; Durack and Wijffels 2010). Such a freshening has also been

observed in the upper layer of the Okhotsk Sea (Hill et al. 2003; Ohshima et al. 2014). On the other hand, the stronger wind-driven circulation leads to enhancement of DSW transport through both an increase in DSW density (caused by the northward transport of the saline water from the Pacific) and an increase in DSW transport from the shelf to the interior (Matsuda et al. 2009; Sasajima et al. 2010).

As described above, sea ice production, freshening of the upper ocean, and the wind-driven ocean circulation are thought to affect the properties of DSW and the OSIW. However, the contributions of these different causes on the multidecadal-scale warming of the OSIW remain unclear. In this study, we conduct a model-based hindcast experiment of the ocean circulation in the western subarctic region including the Okhotsk Sea with interannually varying atmospheric forcing, and evaluate the contribution of the thermohaline and the wind-driven ocean circulation to the warming processes occurring in the intermediate water.

This paper is organized as follows. The model and experimental setting are described in section 2. In section 3, the climatological representation of the model simulation is evaluated in comparison with observational data. In section 4, we compare the simulated and observed OSIW with an emphasis on the multidecadal-scale warming of potential temperature, and conduct perturbation experiments to clarify the major causes of the warming. We also explore the physical process of the warming, and examine the atmospheric forcing pattern related to the multidecadal-scale change. Section 5 presents a summary and discussion.

2. Description of model, experimental setting, and observational data

a. Model

The ice–ocean coupled model used in this study is the Center for Climate System Research Ocean Component Model coupled with a sea ice model (COCO v3.4) (Hasumi 2006). The settings used for the model simulation are identical to those of Uchimoto et al. (2011, 2014), but with different atmospheric forcing and tidal mixing parameterization. The ocean model solves the primitive equation system under Boussinesq and hydrostatic approximations, and uses a σ_θ–z hybrid vertical coordinate with the free surface. The sea ice model is based on a two-category thickness representation, zero-layer thermodynamics (Semtner 1976), and dynamics with elastic-viscous-plastic rheology (Hunke and Dukowicz 1997). There are 51 levels in the vertical direction with thickness increasing to the deep layers (27 layers from the surface to 500-m depth), the horizontal resolution is 0.5° × 0.5°, and the model domain covers the Okhotsk Sea and the western subarctic gyre region (Fig. 1a).

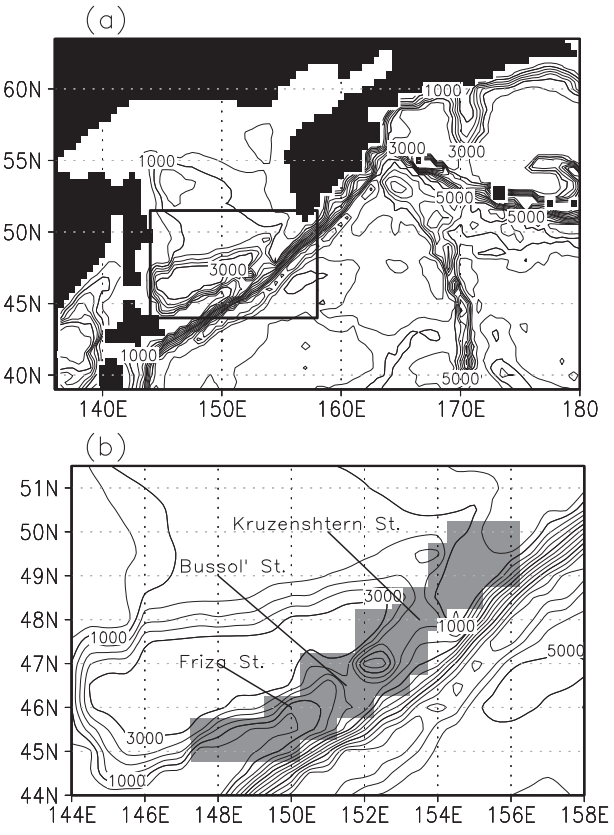

FIG. 1. (a) Model topography. Contour interval is 500 m for depths >1000 m. (b) Model topography around the Kuril Straits [rectangular region in (a)]. Shading indicates region where the tidal mixing parameterization is applied.

The model adopts a third-order advective scheme for tracer equations. The algorithms for horizontal and vertical advection are UTOPIA (Leonard et al. 1995) and QUICKEST (Leonard 1979), respectively. The subgrid-scale mixing due to baroclinic eddies are parameterized by isopycnal diffusion (Cox 1987) and thickness diffusion (Gent and McWilliams 1990), with coefficients of $0.1 \times 10^7\,\mathrm{cm^2\,s^{-1}}$ and $0.3 \times 10^7\,\mathrm{cm^2\,s^{-1}}$, respectively. A shear-dependent viscosity coefficient is used for horizontal viscosity (Smagorinsky 1963), and for vertical viscosity and diffusivity a level-2.5 turbulent closure scheme (Noh and Kim 1999) is applied to all layers. Vertical convection due to unstable stratification is parameterized by the enhancement of vertical diffusivity.

Sponge layers are applied as boundary conditions where temperature and salinity are strongly restored to values of the *World Ocean Atlas 2001* (*WOA2001*) (Stephens et al. 2002; Boyer et al. 2002) with a 1-day restoring time at the edge of the model boundary. Sea

TABLE 1. List of sensitivity experiments.

Experiment	
K_z-W	One-third of K_z ($\sim$6.7 cm s^{-2})
K_z-S	Three times K_z (60 cm s^{-2})
WFLX-O	Evaporation (OAFlux) and precipitation (CMAP)

surface height at the boundary is restored to the climatological sea surface height, which is derived from data of the North Pacific governed by the same configurations as our model, with a 45-min restoring time.

To evaluate the effect of the ventilation induced through the brine rejection of sea ice formation, the SSS is not restored to the climatological value in the simulation. It should be noted that the drift of SSS in the model domain is one order less than the multidecadal-scale change focused in this study. In regions deeper than about 2000 m, temperature and salinity are restored to values of the *WOA2001* with a 10-day restoring time, to reduce the spinup time of the abyssal circulation.

To represent the effects of tidal mixing along the Kuril Straits, we increase vertical diffusivity coefficients (K_z). Since tide-induced diapycnal mixing is essentially important over the sills of the Kuril Straits (which lie at depths of several hundred meters; Nakamura and Awaji 2004, Tanaka et al. 2010), we adopt a constant K_z of 20 cm^2 s^{-1} in the Kuril Straits from the surface to a depth of 500 m (Fig. 1b). This value is comparable to the diapycnal diffusivity estimate averaged over the whole area of the Kuril Straits based on a barotropic tide model (Tanaka et al. 2010). To check the sensitivity of K_z adopted in this study on the model simulation, we conducted simulations using K_z of 6.7 and 60 cm^2 s^{-1} in the Kuril Straits (1/3 and 3 times the standard case, respectively) (Table 1).

b. Experimental setting

The model was first integrated for 50 years from the initial condition based on the climatological temperature and salinity of *WOA2001*, under surface forcing of the climatological monthly-mean NCEP–NCAR reanalysis data from 1979 to 2008 (Kalnay et al. 1996). In the present model, turbulent sensible and latent heat fluxes were computed using bulk formulas with the transfer coefficients of Kara et al. (2000), and radiation fluxes were given as the sum of net solar and longwave radiation fluxes. Freshwater fluxes were estimated from the evaporation minus precipitation of the NCEP–NCAR reanalysis data and the monthly climatology of river runoff data (Dai and Trenberth 2002).

According to Nakanowatari et al. (2010), NCEP–NCAR reanalysis reveal a significant warm bias in the wintertime surface air temperature over the Okhotsk Sea by $\sim$5°C before 1979. An examination of the sea ice extent indicates that there is a significantly larger fraction of open water before 1979 than after this date. However, this is likely to be related to the deficiency of sea ice data in the Okhotsk Sea before 1979, as satellite-derived sea ice concentration data were not available for this period. The model is therefore interannually forced from 1979 to 2008 after the initial 50-yr spinup, and the experiment is hereafter defined as a hindcast experiment.

TABLE 2. List of perturbation experiments.

Experiment	Variables with interannual variations
HEAT	Turbulent heat flux
HEAT-T	Surface air temperature (in the calculation of turbulent heat flux)
HEAT-Q	Specific humidity (in the calculation of turbulent heat flux)
HEAT-W	Scalar wind (in the calculation of turbulent heat flux)
WFLX	Freshwater flux (precipitation − evaporation)
WFLX-P	Precipitation
WFLX-E	Evaporation
WSTR	Wind stress

To evaluate the contribution of each forcing, perturbation experiments were performed in which the interannual variations in atmospheric forcing were restricted to turbulent heat flux (HEAT), freshwater (precipitation minus evaporation) flux (WFLX), and wind stress (WSTR) (Table 2). In each experiment, the other atmospheric forcings were applied by the monthly mean climatological value from 1979 to 2008. In the HEAT experiment, the interannually varied atmospheric variables were surface air temperature, specific humidity, and scalar wind used in the bulk formula. In this case, the wind stress is constant to the climatological monthly mean. For the WSTR, the scalar wind used for the bulk formula is constant to the climatological monthly mean.

Although the duration of the hindcast experiment (1979–2008) is shorter than the period analyzed by Nakanowatari et al. (2007) (1955–2004), the warming signal in the Okhotsk Sea has only been remarkable since the 1970s, and we therefore consider that the period employed within the study covers the essential time period. In addition, the duration used for the simulation covers a somewhat longer period than that of the bidecadal fluctuation observed in the Okhotsk Sea (Osafune and Yasuda 2006). It should be noted that the data in 1979 were not used to avoid initial shock of the simulation.

The Amur River has a watershed area comparable to that of the Okhotsk Sea, and it was thus expected that river runoff would have a substantial contribution to the change in freshwater flux. However, a significant change was not found in the time series of Amur River runoff from 1980 to 2001 (Tachibana et al. 2008), and thus the

effect of interannual variability of river runoff was not accounted for in our simulation.

Since the freshwater flux are not directly assimilated in the reanalysis data, the reanalysis precipitation and evaporation data may contain larger bias compared with the wind speed and surface air temperature (Kalnay et al. 1996), although values are qualitatively consistent (Minobe and Nakanowatari 2002; Serreze et al. 2005). To assess our simulation based on the reanalysis evaporation minus precipitation ($E - P$) data, we conducted the hindcast experiment using the observed $E - P$ products from the OAFlux (Yu and Weller 2007) and CMAP data in which the reanalysis precipitations were not incorporated (Xie and Arkin 1997) (Table 1).

c. Observational data

To evaluate the climatological features and multidecadal-scale change in the model results, we used the isopycnal grid dataset produced by Nakanowatari et al. (2007). This dataset is based on oceanographic observations archived in the World Ocean Database 2001 (WOD01; Conkright et al. 2002) and the Japan Oceanographic Data Center (2003). It is also based on results from the Japan–Russia–United States international joint study of the Okhotsk Sea from 1998 to 2004 (Ohshima et al. 2004; Itoh 2007; Ohshima et al. 2010), and profiling float data obtained by the international Argo program from 2000 to 2004 (Argo Science Team 2001) (herein referred to as WOD01+).

The quality control and gridded method adopted in this study is similar to those of earlier studies (Itoh et al. 2003). Hydrographic data at discrete depths, mostly from bottle samples, were linearly interpolated to 1-m interval, and then the values of the potential temperature, salinity, isopycnal layer thickness, and isopycnal depth were selected at $0.1\sigma_\theta$ intervals from $(26.6–27.1)\sigma_\theta$. The isopycnal layer thickness is defined here by the distance between the isopycnal surfaces with densities $0.05\sigma_\theta$ higher and lower than the specified density (i.e., $h(\sigma_\theta) = z(\sigma_\theta + 0.05) - z(\sigma_\theta - 0.05)$, where z is depth.

Before we applied a quality control, we divided all of the data into two parts, one set for the Okhotsk Sea and the other for the Pacific Ocean, because the water mass properties differ considerably between the two oceans. To perform the quality control check, the data were first divided into 60-km geographical squares. Within each geographical bin, the mean and the standard deviation of the potential temperature, salinity, isopycnal layer thickness, and depth were calculated. Then, data that fell outside the 2.5 interval were eliminated. The above quality check procedure was further performed for larger geographical bins, specifically by using 200-km and 400-km geographical squares.

Annual mean climatology was calculated using a $0.25° \times 0.25°$ latitude/longitude grid, with a method similar to that of Levitus and Boyer (1994). To calculate a grid value of the annual mean climatology from the station data, we used the Gaussian distribution as a weight function with an e-folding scale of 75 km and an influence radius of 150 km to resolve regional features in the Okhotsk Sea and the boundary current. An e-folding scale of 75 km can be fit to the autocorrelation functions on each isopycnal bin in and around the Okhotsk Sea (Itoh et al. 2003). If the number of observations within the influence radius was less than 5, that grid box was regarded as having no data. Annual mean anomalies were gridded using simple averaging of anomalies as the differences of the observed values from the climatologies, over a yearly $2.5° \times 2.5°$ grid box from 1970 to 2004. Neither spatial interpolation nor spatial smoothing was applied to the anomaly field.

To validate the simulated temperature variability in the OSIW, we also used the historical time series of annual potential temperature on isopycnal surfaces averaged over the Kuril basin, which is defined by the region deeper than 2000 m in the Okhotsk Sea (Fig. 1b), produced by Uehara et al. (2012, 2014). This time series are based on hydrographic observations archived in the Far Eastern Regional Hydrometeorological Research Institute (FERHRI) database and are available from 1951 to 2006. Since the monthly mean climatological values were removed before the annual anomalies were calculated, the effect of seasonal variation is subtracted in the time series. To evaluate the multidecadal-scale change of the potential temperature in the OSIW, we used the time series from 1970 to 2006.

To validate the simulated sea ice production, we used ice production estimated by a heat budget analysis using ice concentration, thickness, and drift speed from satellite observation, and Interim ECMWF Re-Analysis (ERA-Interim) data (Nihashi et al. 2012) (available from 2003 to 2009 with a spatial resolution of 12.5 km). In their study, ice production rate per unit area (V_i) in the Okhotsk coastal polynyas is calculated by $V_i = Q/\rho_i L_f$, where Q is daily heat loss from the sea surface to the atmosphere, ρ_i ($=920\,\mathrm{kg\,m^{-3}}$) is the density of ice, and L_f ($=0.334\,\mathrm{MJ\,kg^{-1}}$) is the latent heat of fusion for ice. In this calculation, oceanic heat flux due to the circulation and eddy mixing is assumed to be negligible, because this method is only applied to the coastal polynya regions. Sea ice concentration data were derived from the Hadley Centre Sea Ice and Sea Surface Temperature dataset version 1 (HadISST; Rayner et al. 2003), and climatological monthly means were calculated using the period 1979–2008.

The altimeter data derived from the merged products of monthly mean sea surface height anomaly (SSHA)

from TOPEX/Poseidon, *Jason-1*, and European Research Satellite altimeter observations were used for the representation of the simulated ocean circulation change. The sea level anomalies are produced by the French Archiving, Validation, and Interpolation of Satellite Oceanographic Data (AVISO) project using the mapping method of Ducet et al. (2000).

3. Climatological features of the model

In this section, we compare climatological fields from the hindcast data with previous estimates from observational data, to assess simulated sea ice production, the water property of the intermediate layer, and ocean circulation.

a. Sea ice production

Figures 2a and 2b compare spatial patterns of annually accumulated freshwater flux related to sea ice production and/or melting within the observational and simulated data. For the observational data, the freshwater flux related to sea ice melting is calculated with some assumptions (e.g., constant ice thickness of 0.34 m is made for all melting ice; for details, see Nihashi et al. 2012). The simulated freshwater fluxes related to ice production (or melting) are calculated from the input of freshwater from ocean to sea ice (or from sea ice to ocean). Prominent positive values along the northern and northwestern shelf are a common feature in both data sets, indicating that a large amount of sea ice production in the coastal polynya is qualitatively represented in the model. The rate of simulated sea ice production over the northwestern shelf region (the rectangular region shown in Fig. 2b) is $4.3 \times 10^{11}\,\mathrm{m^3\,yr^{-1}}$, which is somewhat smaller than the observed estimate of sea ice production rate of $6.5 \times 10^{11}\,\mathrm{m^3\,yr^{-1}}$ (Nihashi et al. 2012). The model results also show negative values due to sea ice melting in the southern part of the Okhotsk Sea, although the simulated negative region is located near the Kuril Strait compared with the observational estimate. Since the sea ice melts along the sea ice edge region, this might be related to the difference in the location of sea ice edge.

Since the sea surface salinity in the northwestern shelf is also important for the DSW formation, we evaluated the representation of the simulated SSS. Figures 2e and 2f show the annual means of SSS from the observational and simulated data. The simulated SSS in the northwestern shelf region is 32–32.5 psu, which is comparable to the observed SSS. Relatively low SSS along the Sakhalin Island and high SSS along the Kamchatka Peninsula are qualitatively simulated in the model, although the SSS is about 0.5 psu lower than the observed one. On the other hand, the relatively high SSS extending from the subtropical gyre is not simulated. Since it is known that the northeastward quasi-steady jet (Isoguchi et al. 2006) and anticyclonic warm-core rings (Itoh and Yasuda 2010) have a role in the northward transport of saline water, such a mesoscale phenomenon may not be well simulated in this model.

b. Water mass properties

Figures 2c and 2d show spatial patterns of the annually averaged potential temperature at $26.8\sigma_\theta$ for the observation and model, respectively. The observed potential temperature shows that the DSW, which is defined here as a water mass with potential temperature of less than 0°C, is distributed over the northwestern shelf in the Okhotsk Sea (Fig. 2c). This relatively cold water extends southward along the western boundary of the Okhotsk Sea and flows out to the North Pacific through the Bussol' Strait. These features are reproduced in the simulated potential temperature (Fig. 2d). On the other hand, the simulated potential temperature in the eastern part of the Okhotsk Sea is about 1°C warmer than the observational data (Fig. 2d). The fact that the warm and saline water from the North Pacific comes through the northern part of the Kuril Straits from the East Kamchatka Current (EKC; Ohshima et al. 2010) suggests that this warm bias is related to the overestimate of the EKC inflow transport.

In the western North Pacific, the observed subarctic front represented by the contour of 3°C extends northeastward, but the simulated subarctic front extends eastward (Fig. 2d). In this way, in spite of these geographical differences between the observed and simulated climatologies of the potential temperature at isopycnal surface, the cold and freshwater originated from the DSW and its outflow to the North Pacific are qualitatively simulated.

c. Isopycnal layer thickness

Since the OSIW is characterized by low potential vorticity (i.e., volumetric mode water) at the intermediate depths, simulated layer thickness at this isopycnal surfaces is compared with the observed one. The isopycnal layer thickness is defined here as the two isopycnal surfaces with a specified density $\pm 0.05\sigma_\theta$. Figure 3a shows the vertical–meridional section of observed layer thickness along 148°E, where σ_θ is used as the vertical axis. A relatively thick layer corresponding to the OSIW is found in the intermediate layer [$(26.7–27.0)\sigma_\theta$], and the maximum layer thickness is found near the Kuril Straits (45°N), implying that vertical mixing by tidal current locally modifies the water mass structure. The distribution of simulated layer thickness is similar to

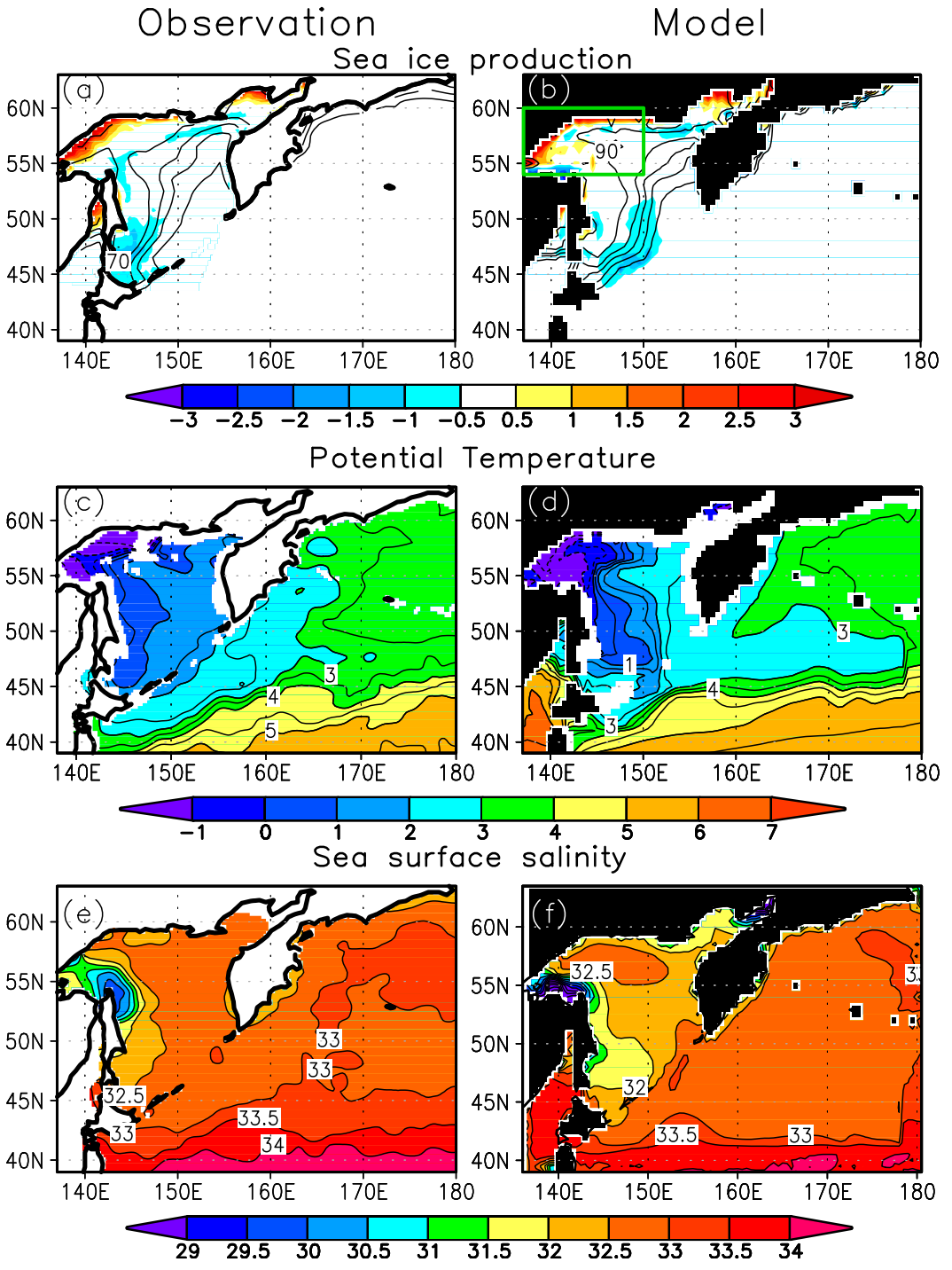

FIG. 2. (a) Observed and (b) simulated (hindcast) climatologies of the annual freshwater flux (m yr^{-1}) associated with sea ice production (positive) and melting (negative). Climatological sea ice concentrations in February are superimposed. Contour interval is 10%, 30%, 50%, 70% and 90%. (c) Observed and (d) simulated (hindcast) climatologies of annually averaged potential temperature (°C) at 26.8σ. (e),(f) As in (c),(d), but for sea surface salinity (psu).

that of the observed (Fig. 3b), although the core density of the OSIW is 0.1σ_θ heavier than that of observations. The difference of the isopycnal layer thickness in the observed and simulated data is confined near the Kuril Straits (46°–48°N) and on the isopycnal surfaces lighter than 26.8σ_θ. Therefore, the cause of the density difference in this region may be related to the insufficient tidal mixing processes (Nakamura et al. 2000a,b), because we

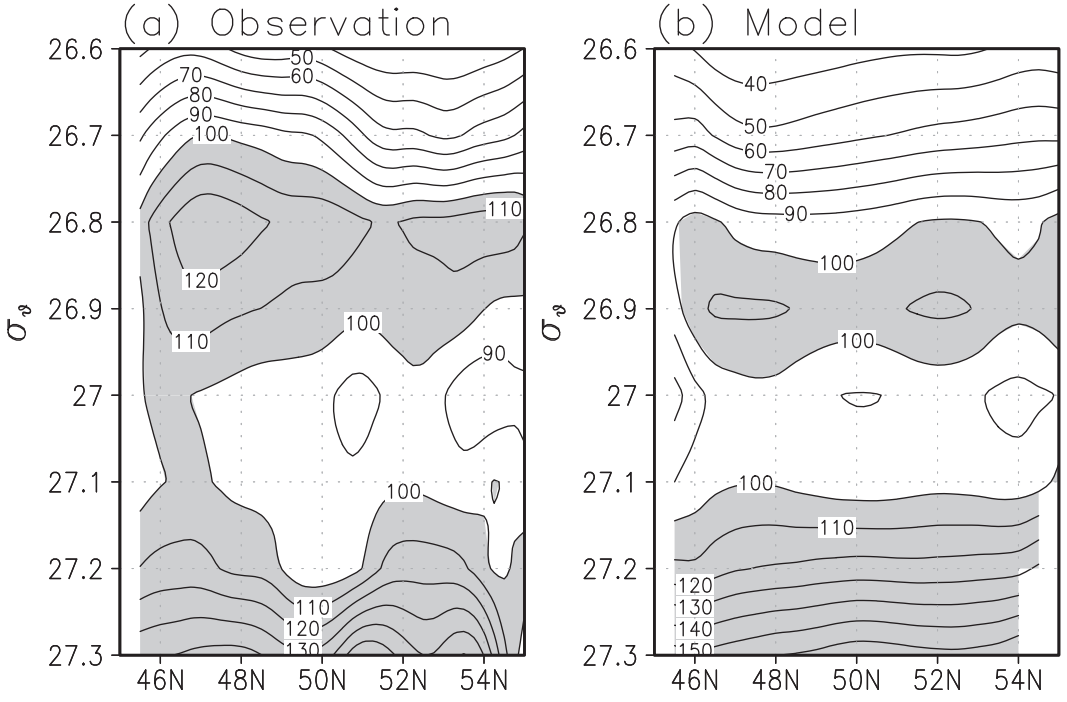

FIG. 3. The latitudinal cross section of the climatological layer thickness (m) along 148°E derived from the (a) observation and (b) model. The vertical axis is potential density. The shading indicates the regions where the thickness is >100 m.

adopt this effect in a simple way [the enhanced temperature–salinity (*T*–*S*) vertical diffusive coefficients along the Kuril Straits]. Since we focus on the potential temperature change in the density range of (26.9–27.1)σ_θ [the densities heavier than the core density of (26.7–26.8)σ_θ], such a difference is not important for our study.

4. Results

a. Simulated warming of potential temperature

We begin by examining the spatial pattern of multidecadal-scale warming at 27.0σ_θ, where the maximum rate of warming is observed in the Okhotsk Sea (Itoh 2007). For the evaluation of warming signal, we calculated the linear trend of potential temperature on isopycnal surfaces. Since the warming is remarkable since 1970s, we used the WOD01+ data from 1970 to 2004 to show the statistically significant warming signal in the potential temperature in and around the Okhotsk Sea.

Observed warming trends in this period are statistically significant along the western part of the Okhotsk Sea and the western subarctic front as shown by Nakanowatari et al. (2007) (Fig. 4a). The hindcast experiment shows the significant warming trends along the Sakhalin Island and the western subarctic front, which are similar to the observed trend patterns (Fig. 4b). On the other hand, the simulated potential temperature shows the cooling in the eastern part of the Okhotsk Sea. Since the climatological potential temperature in this region is not well simulated (Fig. 2d), this might be related to the model bias. In addition, the observed warming in the western subarctic front is slanted to northeast, whereas the simulated warming is essentially eastward. Despite these geographical differences between the warming trends in the simulation and observations, the significant warming in the OSIW and the western subarctic front are qualitatively simulated.

Figure 5a compares the observed and simulated vertical profiles of the linear trend in the potential temperature averaged in the western Okhotsk Sea (region A shown in Figs. 4a and 4b) in which the warming trends are significant in the observation and simulation. The warming trends calculated from WOD01+ data are 0.2°–0.3°C $(30\,\text{yr})^{-1}$ in the density range of (26.8–27.2)σ_θ, and statistically significant at 90% confidence level. The similar results are also obtained from the FERHRI dataset. The simulated trends also show the significant warming in the corresponding density range, but the absolute values are relatively large at (26.9–27.0)σ_θ, compared with those observed.

Figure 6a shows the time series of the annually averaged potential temperature anomalies averaged over the western part of the Okhotsk Sea (region A) at 27.0σ_θ for the observed (WOD01+ and FERHRI) and hindcast

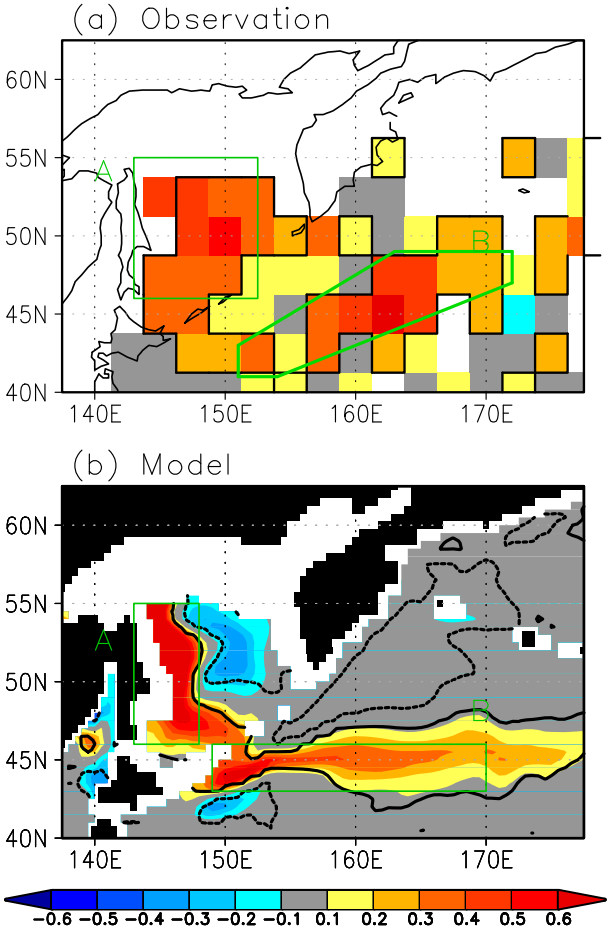

FIG. 4. Linear trend maps [°C (30 yr)$^{-1}$] in the annually averaged potential temperature at 27.0σ_θ in (a) observed data from 1970 to 2004 and (b) the hindcast experiment from 1980 to 2008. The white-colored regions in (b) represent water that is lighter than the corresponding density. The contour indicates the regions where the linear trend is significant at 90% confidence level. The significance of the linear trend estimate is based on a Student's t distribution.

data, where an anomaly is defined as a deviation from the climatological mean. The observed potential temperature anomalies in both datasets show the gradual warming trend since 1970s with decadal fluctuations with negative anomalies in 1970s and 1990s and positive anomalies in 1980s and 2000s. The observed anomalies in the two datasets are highly correlated with each other ($r = 0.84$), indicating that these interannual variations are reliable. The time series of the hindcast data also exhibit a warming trend and similar decadal fluctuations, but the warming trend is overestimated and the correlation between the simulated and observed potential temperature is not so high ($r = 0.46$). This might be partly related to the unrealistic negative anomaly of the simulated time series in late 1980s. Osafune and Yasuda (2006) pointed out that the potential temperature anomaly in this period is positive from the observational data and suggested the influence of the 18.6-yr period nodal cycle. Thus, the absence of the positive anomaly may be related to the fact that the strength of the tidal mixing is constant in the hindcast experiment.

In the western subarctic front region (region B in Figs. 4a,b), the vertical distribution of the observed linear trend indicates that the potential temperature has significantly warmed in the entire density range from 27.2σ_θ to 26.7σ_θ (Fig. 4b). The warming trend strengthens with decreasing depth. The simulated warming trends are within the range of the 90% confidence interval of the observed warming trends. The time series of both the observed and simulated potential temperature averaged over region B shows the gradual warming since 1970s and the decadal fluctuations with positive anomalies from 1975 to 1985 and from 1995 to 2000, and negative anomalies from 1985 to 1995 (Fig. 6b). The correlation between the simulated and observed potential temperature anomalies is 0.70 at 27.0σ_θ, with no time lag. On the other hand, the abrupt occurrence of positive anomalies in 2000 (approximately) is not present in the hindcast data. This could be related to the inadequate spatial resolution, which is not fine enough to resolve the quasi-stationary jet that transports warm waters across the transition zone from the subtropics to the subarctic (the strength of the jet is connected to the northward shift of Kuroshio Extension for 1999–2002) (Isoguchi et al. 2006). Thus, in spite of some discrepancy between the observed and simulated variations in the potential temperature, the warming trends in the Okhotsk Sea and western subarctic front are qualitatively represented in this simulation.

We also validate the simulated warming trends in the Okhotsk Sea and western subarctic front from the comparison with the sensitivity experiments on the freshwater fluxes (WFLX-O) and the vertical diffusivity coefficients (K_z-W and K_z-S; Table 1). Figure 7 shows the trend map of the potential temperature at 27.0σ_θ from the sensitivity experiments. The significant warming trends along the Sakhalin Island and the western subarctic front are represented in these sensitivity experiments, although their magnitudes are somewhat modified. The vertical distributions of the linear trend also shows the warming trends in the Okhotsk Sea and subarctic frontal region, which are significant at 90% confidence level in the intermediate layer [(26.9–27.1)σ_θ] in these sensitivity experiments (Fig. 8). However, the warming of the OSIW in the WFLX-O is ~0.2°C (30 yr)$^{-1}$ at (26.9–27.0)σ_θ, which is about 3 times less than the original hindcast experiment. This result suggests that the freshwater flux change in the OSIW may be overestimated in the hindcast experiment. The

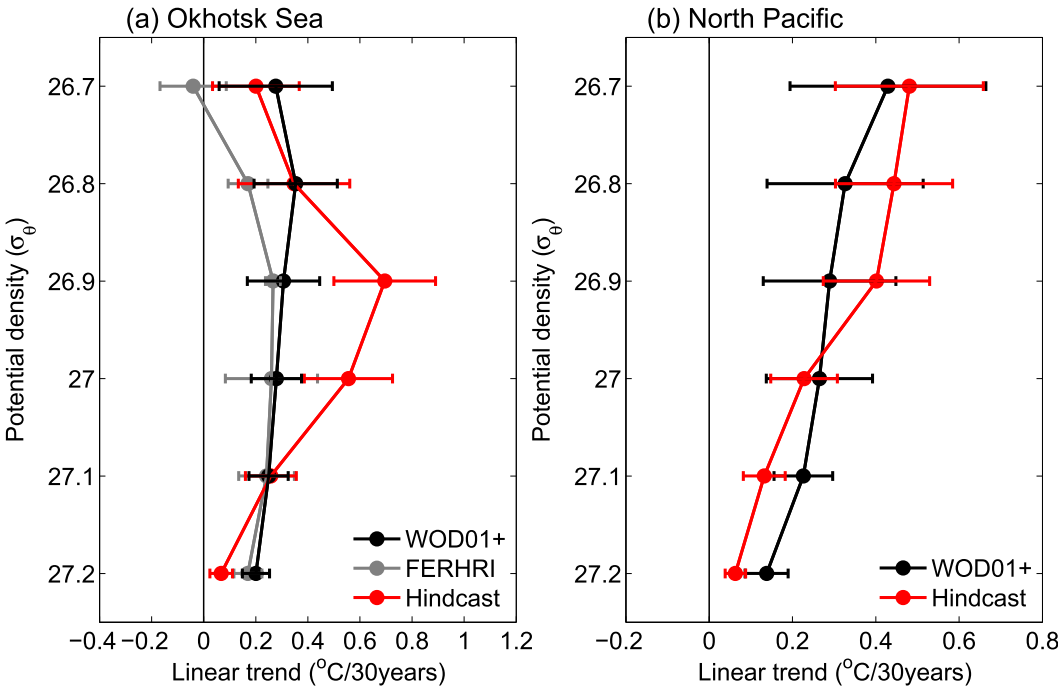

FIG. 5. Linear trends of the annually averaged potential temperature on isopycnal surfaces from the WOD01+ (black), FERHRI (gray), and hindcast data (red), averaged over (a) the western part of the Okhotsk Sea (region A) and (b) the western subarctic North Pacific (region B). The error bars indicate the 90% confidence interval for the linear trend estimate.

warming trends of the OSIW in K_z-S and K_z-W are also significant at 90% confidence level, indicating that the sensitivity of the K_z value is not so large on the warming trend of the OSIW. It is noted that the warming trends of the subarctic frontal region at (26.9–27.0)σ_θ in K_z-S is smaller than those in K_z-W. This result is explained by the fact that the tidal mixing affects the outflow rate from the Okhotsk Sea as well as the strengthened ventilation over the northwestern shelf (Matsuda et al. 2009).

The present model does not include wind stress variations east of 180°E, and this could be a reason for the underestimation of the warming trend in the western subarctic front. However, it should be noted that the baroclinic Rossby waves excited over the eastern basin are expected to be damped before reaching the area considered here, because the dumping time scale for the first mode baroclinic Rossby waves (~6 yr) is shorter than the time required for the waves to travel across the subarctic North Pacific (~15 yr) (Qiu 2002). In addition, barotropic Rossby waves are blocked by the Emperor Sea Mounts (Kono and Kawasaki 1997; Ito et al. 2004; Nonaka et al. 2008).

To check the validity of the above assumption, we evaluated the representation of the ocean circulation variability in the simulated data by comparing it with the altimeter data. For the strength of the East Kamchatka Current in the western subarctic gyre, we used the EKC index, which is defined by the difference in SSHA between the east Kamchatka coast (53°N, 160°E) and its offshore area (50°–55°N, 165°–170°E), according to Ohshima et al. (2010). Figure 9 shows the time series of the annual mean EKC index calculated from the simulation and observations. The simulated data well captures the interannual variability in the EKC with remarkable positive anomalies in 2004–05 and negative anomalies in 1998 and 2006–08. The correlation between the observed and simulated EKC indexes is 0.78 from 1994 to 2008 and is significant at 99% confidence level based on the Monte Carlo simulation with a phase randomization technique generating 1000 surrogate time series (Kaplan and Glass 1995). This comparison supports that the interannual variation of the subarctic gyre is well represented in the model simulation. Thus, although the effect of the wind stress in the east is not accounted in our experiment, it is considered meaningful to examine the simulated warming trend in the western subarctic front, where the simulated potential temperature is highly correlated with the observed one.

b. *Causes of the warming trend*

To clarify the causes of the simulated warming trends in the Okhotsk Sea and the western subarctic front, we

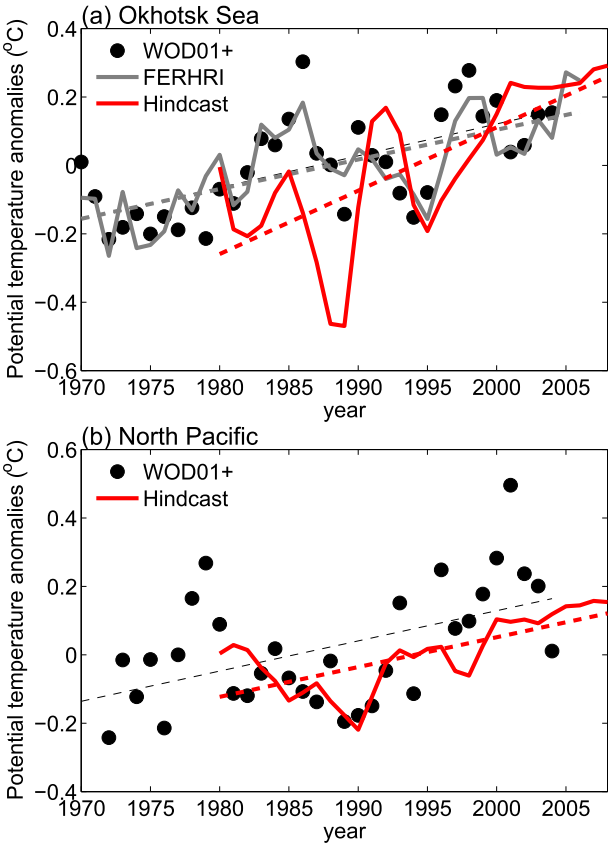

FIG. 6. Time series of the annual mean of potential temperature anomalies averaged over (a) the southern part of the Okhotsk Sea (region A) and (b) the western subarctic North Pacific (region B), at 27.0σ_θ for the WOD01+ (black circles), FERHRI (gray line), and hindcast data (red line). Linear regressions of the annual time series are indicated by dashed lines.

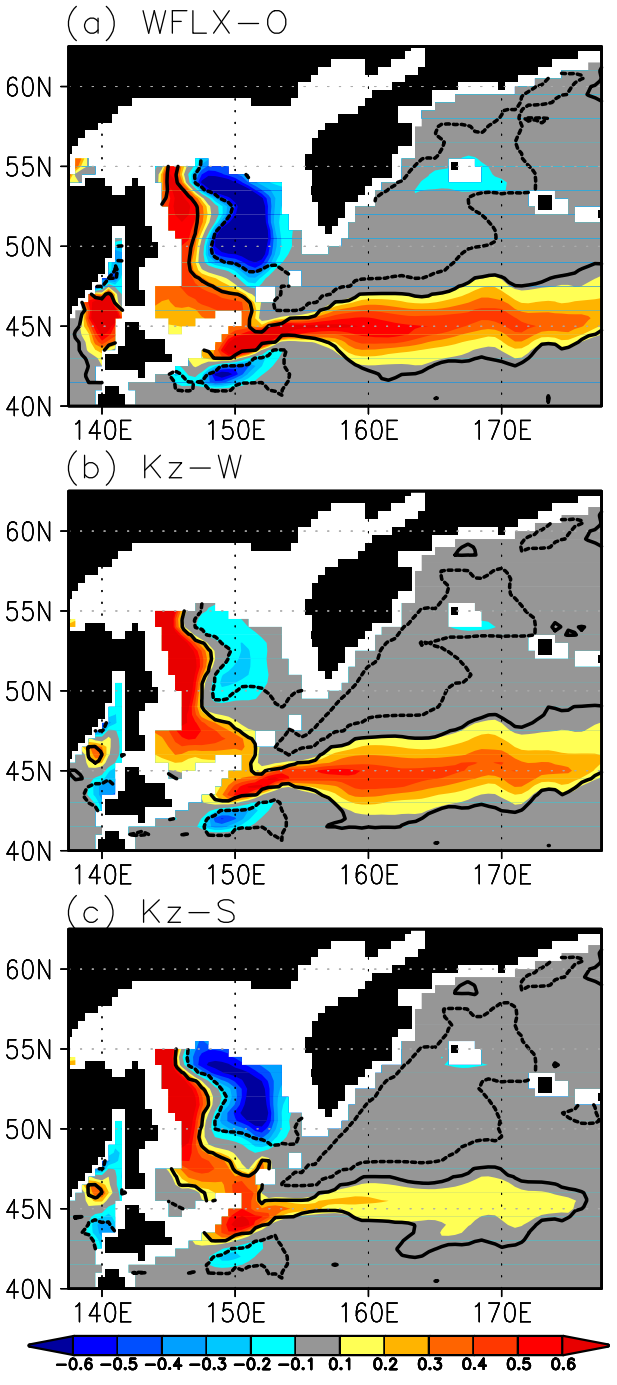

FIG. 7. As in Fig. 4b, but for the sensitivity experiments of (a) WFLX-O, (b) K_z-W, and (c) K_z-S.

examined perturbation experiments using turbulent heat flux (HEAT), freshwater flux (WFLX), and wind stress (WSTR). Figure 10 shows the linear trend maps of potential temperature at 27.0σ_θ in the perturbation experiments, and it is evident from these that the turbulent heat and freshwater fluxes cause the warming in the potential temperature in the Okhotsk Sea (Figs. 10a,b). The warming trends are seen to be relatively large along the pathway of the DSW, and a part of the warming signal extends to the North Pacific via the Bussol' Strait. In contrast, however, the wind stress variation causes a cooling trend in the OSIW (Fig. 10c).

Figure 11a shows the time series of the annual mean of potential temperature anomalies averaged over the western part of the Okhotsk Sea at 27.0σ_θ for perturbation experiments. The potential temperature anomalies in the HEAT experiment are characterized by the gradual increase trend with the decadal fluctuations with negative anomalies in 1980s and 2000s and the positive anomalies in 1990s. The warming trend in the WFLX is related to the multidecadal variability with the negative anomalies from 1980s to 1990s and the positive anomalies in 2000s. On the other hand, the cooling trend in the WSTR experiment is marked by a significant negative anomaly in late 2000s. Thus, the positive anomaly of the

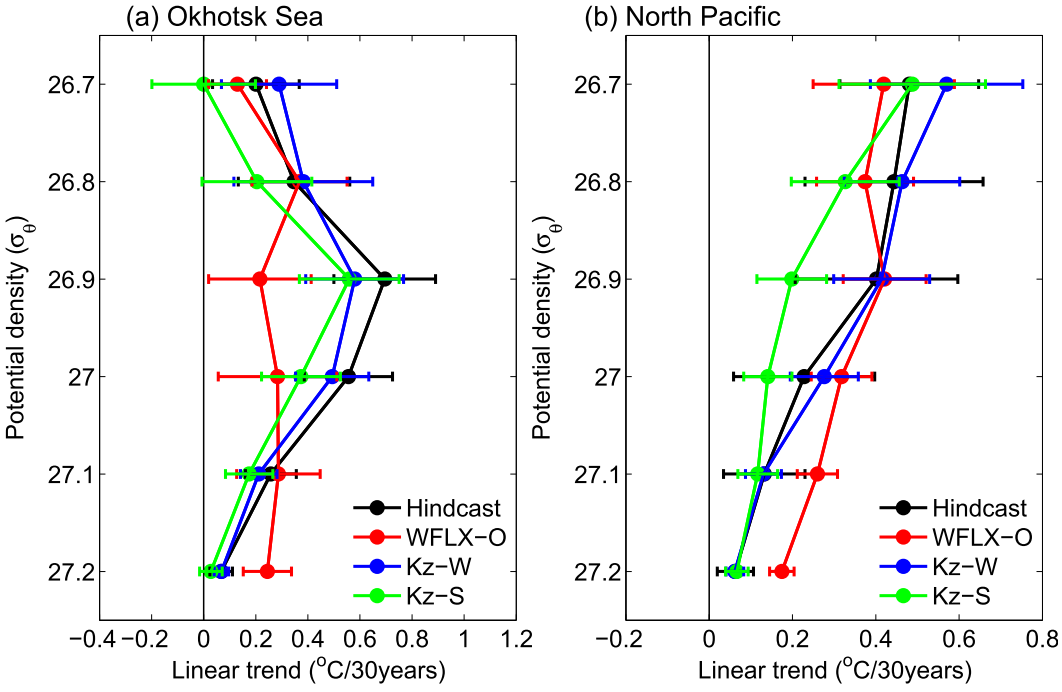

FIG. 8. As in Fig. 6, but for the annually averaged potential temperature on isopycnal surfaces from the hindcast data (black), the WFLX-O (red), K_z-W (blue), and K_z-S (green).

simulated potential temperature in OSIW since 2000 (Fig. 6a) cannot be explained only by the heat and wind stress change.

In the subarctic frontal region, all of the turbulent heat flux, freshwater flux, and wind stress forcings positively contribute to the warming trend at 27.0σ_θ (Fig. 10). In particular, the warming trend in the WSTR is largest in these experiments and extends eastward from the Kuril Strait. The time series of the potential temperature anomalies averaged over the subarctic frontal region indicate that the warming trend in the WSTR is evident for the simulation period (Fig. 11b). For the HEAT and WFLX experiments, the potential temperature variations in the subarctic region are similar to those in the Okhotsk Sea, although the former lags the latter by 2 or 3 yr (Fig. 11b). These results imply that the potential temperature anomaly in the OSIW is advected to the subarctic region along the isopycnal surface.

The linear trend of the potential temperature at 27.0σ_θ for the residual components, which is the difference between the hindcast data minus the sum of the HEAT, WSTR, and WFLX experiments, partly contributes to the warming trend within the Okhotsk Sea with 0.1°–0.2°C $(30\,\mathrm{yr})^{-1}$, although the signal is relatively smaller than the HEAT, WSTR, and WFLX experiments (Fig. 10d). This may be related to the nonlinear effects of isopycnal mixing processes between the perturbed forcings. In fact, the relatively large signal is found in the regions where the lateral gradient of the climatological potential temperature is relatively large (Fig. 2d). Thus, the warming trends seen in the hindcast experiment can be essentially explained by the turbulent heat and freshwater fluxes, and the wind stress; the nonlinear effects between these fluxes (and other fluxes) are not essential for the warming trend in the intermediate water temperature.

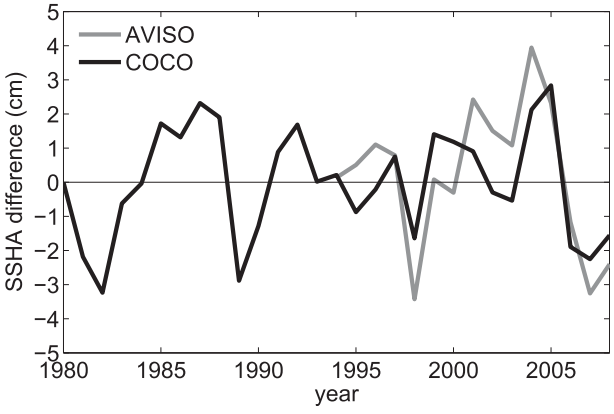

FIG. 9. Time series of the annual mean of EKC index, which is the difference in SSHA between the east Kamchatka coast (53°N, 160°E) and the offshore area (50°–55°N, 165°–170°E) from the altimeter data (gray) and simulated data (black). The positive anomaly means that the EKC is enhanced relative to the climatological value.

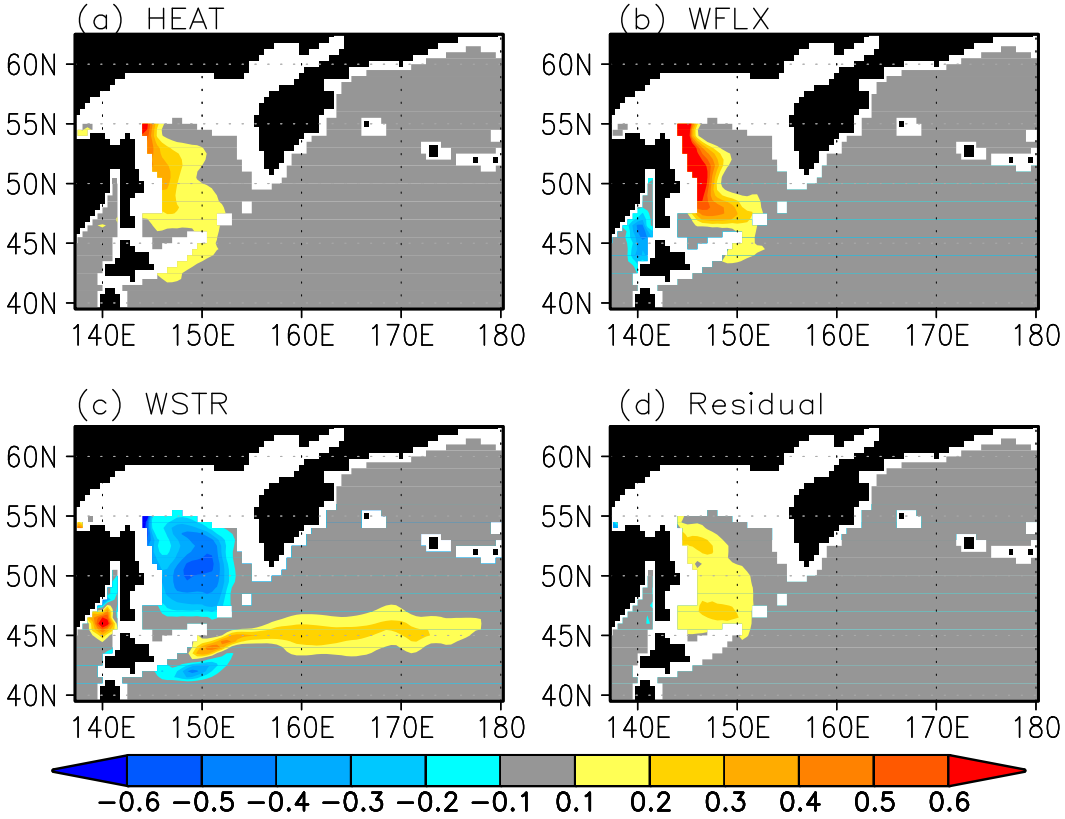

FIG. 10. Linear trends [°C (30 yr)$^{-1}$, colors] in annually averaged potential temperature at 27.0σ_θ, calculated from the (a) HEAT, (b) WSTR, (c) WFLX experiments, and (d) the residual component (the hindcast minus the sum of the HEAT, WSTR, and WFLX experiments). The white regions represent areas where water is lighter than 27.0σ_θ.

c. *Processes responsible for trends: Heat budget analysis*

The perturbation experiments show the contributions of turbulent heat and freshwater fluxes, and of wind stress to the warming trends in the Okhotsk Sea and the western subarctic front. In this section, we examine the potential temperature tendency and the related advection and diffusion terms on the isopycnal surface of 27.0σ_θ to clarify the physical mechanism of the interannual variation forced by each forcing. The potential temperature tendency at the isopycnal surface is given by

$$\frac{\partial \theta|_s}{\partial t} = \mathrm{ADV} + \mathrm{MIX}, \qquad (1)$$

where $\theta|_s$ is potential temperature on the isopycnal surface, ADV represents heat flux convergence owing to large-scale flow, and MIX represents heat flux convergence owing to mixing processes that include effects of subgrid-scale eddies, and isopycnal and diapycnal mixing. We calculated each term on the right-hand side of Eq. (1), and then interpolate it onto the isopycnal surface. Each term in Eq. (1) is regressed onto the time series of annually averaged potential temperature averaged over regions A and B. We examined the heat budget in the HEAT, WFLX, and WSTR experiments for the Okhotsk Sea (region A). On the other hand, for the subarctic frontal region (region B), we investigate the heat budget only in the WSTR experiment, because it is apparent that the warming signal is advected from the Okhotsk Sea in the HEAT and WFLX experiments (Figs. 6a,b).

1) HEAT EXPERIMENT

Figure 12a shows the lagged regressions of annually averaged temperature tendency and the related heat flux convergences onto the potential temperature averaged over the western part of the Okhotsk Sea (region A). Figure 12a indicates that the lag regressions of the temperature tendency reach a maximum at lag −1 to −2 yr. Since the temperature tendency is in phase with the ADV term, the ADV term is highly related to the development of temperature tendency. On the other hand, the regressions of the MIX term are small compared with those of the ADV term in the Okhotsk Sea

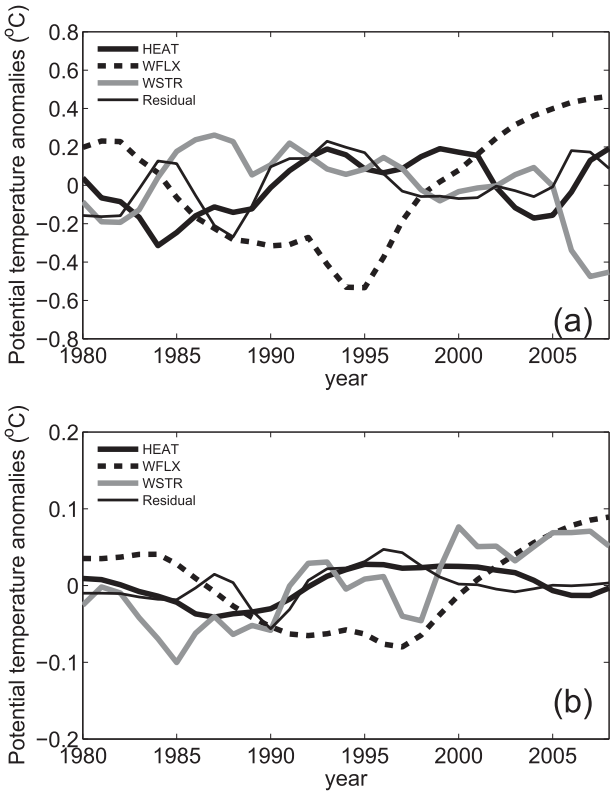

FIG. 11. Time series of the annual mean of potential temperature anomalies at $27.0\sigma_\theta$ over (a) the western part of the Okhotsk Sea (region A) and (b) the subarctic frontal region (region B), derived from perturbation experiments (HEAT, WFLX, and WSTR) and the residual component (the hindcast experiment minus the sum of the perturbation experiments).

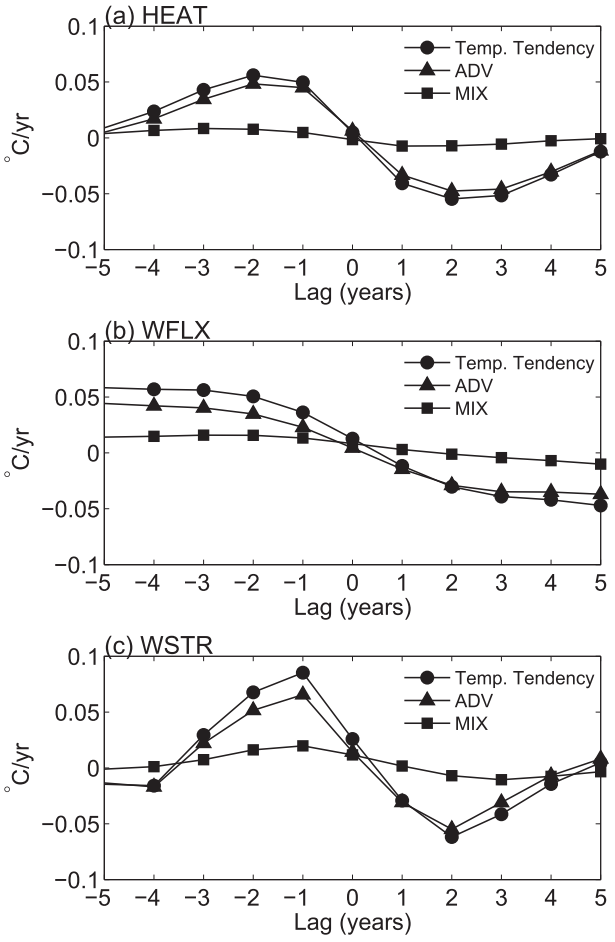

FIG. 12. Lagged regression of annually averaged tendency for the potential temperature (circles) and the convergence of the heat fluxes by large-scale flow (ADV, triangles) and mixing processes (MIX, squares) onto the time series of the potential temperature at $27.0\sigma_\theta$ averaged over the western part of the Okhotsk Sea (region A) in the (a) HEAT, (b) WFLX, and (c) WSTR experiments. The negative values of lag time mean that the tendency leads the potential temperature.

(region A). The regression map of the ADV term at −1-yr lag (Fig. 13a) shows that the positive regression of the ADV term is closely confined to the western part of the Okhotsk Sea. Furthermore, these positive regressions of the ADV term are related to the northward heat flux anomalies. These results suggest that the warming trend in the western part of the Okhotsk Sea in the HEAT experiment is caused by an increase in the advective heat flux convergence related to the weakening of cold DSW transport from the northwestern shelf.

To investigate the cause of the decrease in the DSW transport, we estimated the trend of sea ice production, because only the turbulent heat flux was varied interannually in the HEAT experiment. The sea ice production in this experiment showed a significant negative trend of $-0.63 \times 10^{11}\,\mathrm{m}^3\ (30\,\mathrm{yr})^{-1}$ (Fig. 14a), with a relatively large rate of decrease in March. To evaluate the contribution of each thermodynamic parameter used in the turbulent heat flux calculation to the decrease in sea ice production, we conducted perturbation experiments in which only surface air temperature (HEAT-T), specific humidity (HEAT-Q), and wind speed (HEAT-W) were varied interannually (Table 1). The linear trends of sea ice production over the northwestern shelf in HEAT-T, HEAT-Q, and HEAT-W are −0.66, −0.14, and $0.16 \times 10^{11}\,\mathrm{m}^3\ (30\,\mathrm{yr})^{-1}$, respectively (Fig. 14a). Accordingly, a warming of atmospheric temperature accounts for most of the decrease in sea ice production.

2) WFLX EXPERIMENT

The potential temperature change in the Okhotsk Sea forced by the freshwater flux can be explained by the lateral advection in a similar manner to the HEAT experiment. The lagged regressions of the temperature tendency are positive at lag of −1 to −5 yr, and are

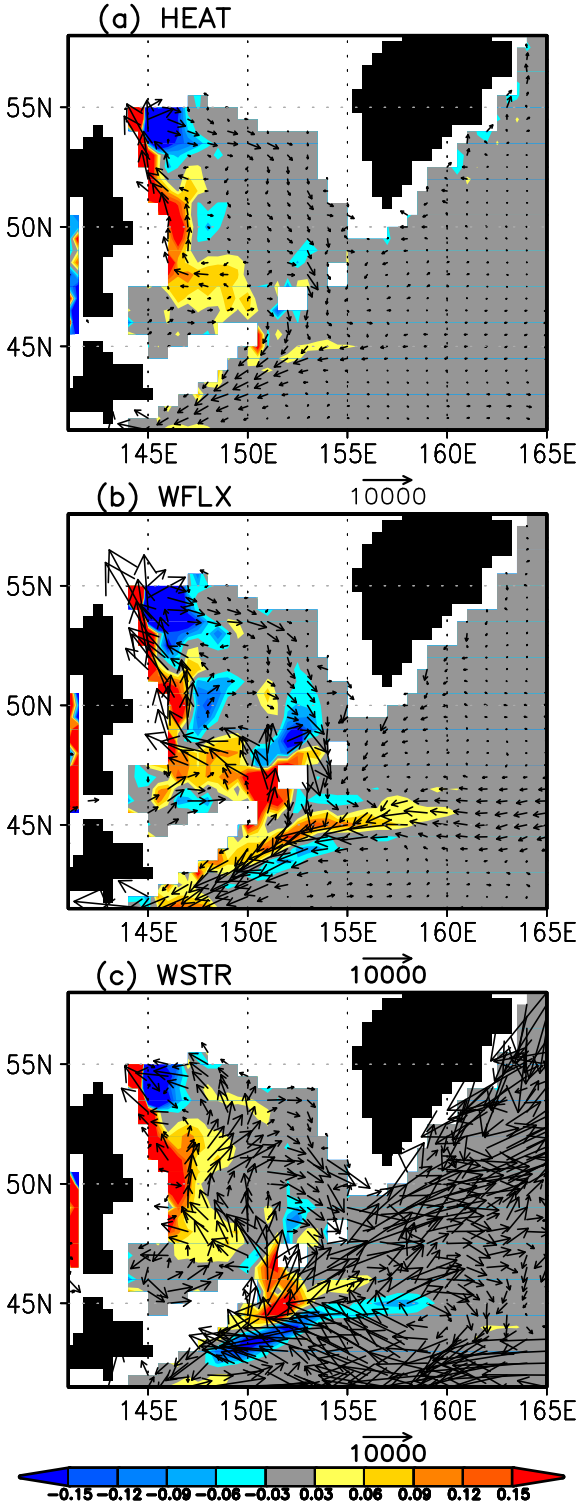

FIG. 13. Lag −1 yr regression maps of annually averaged heat fluxes (vectors, °C m^{-3} yr^{-1}) and their convergence (color shades with positive values, °C yr^{-1}) by large-scale flow (ADV) onto the potential temperature at 27.0σ_θ averaged over the western part of the Okhotsk Sea (region A), calculated from the (a) HEAT, (b) WFLX, and (c) WSTR experiments. The vertical component of the heat flux is not shown. In (c), the signs of the regression coefficients are inverted. The white regions represent areas with water lighter than 26.9σ_θ.

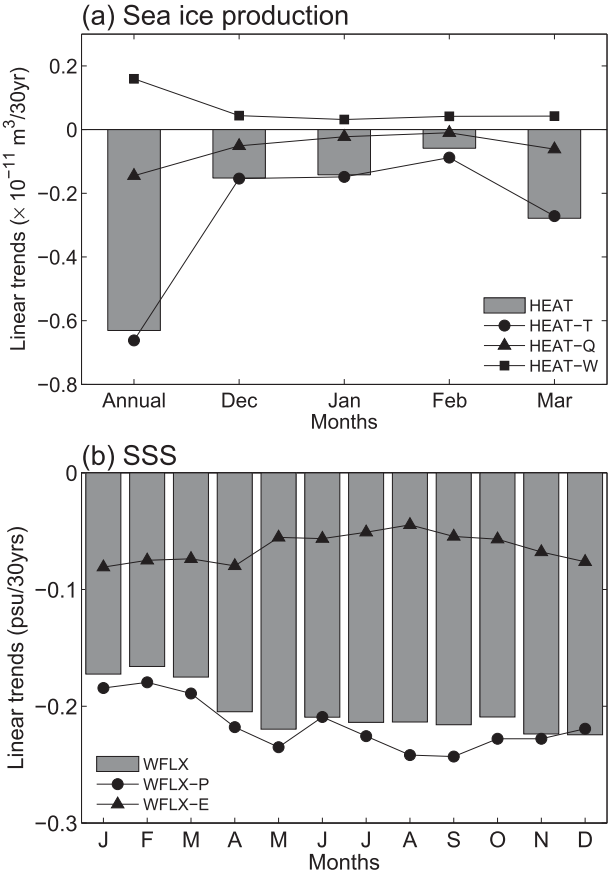

FIG. 14. (a) Linear trends [×10^{11} m^3 (30 yr)$^{-1}$] in the annual and monthly sea ice production in the HEAT (gray bars), HEAT-T (circles), HEAT-Q (triangles), and HEAT-W (squares) experiments. Sea ice production is integrated over the northwestern shelf region (54°–60°N, 137°–150°E). (b) Linear trends [psu (30 yr)$^{-1}$] in monthly sea surface salinity over the northwestern shelf region in the: WFLX (gray bars); WFLX-P (circles); and WFLX-E (triangles) experiments.

almost in phase with those of the ADV term (Fig. 12b), although the peak is not found due to its low-frequency characteristics (Fig. 11a). The regression map of the ADV term at −1-yr lag (Fig. 13b) shows that the positive regression of the ADV term along the western part of the Okhotsk Sea is related to the northward heat flux anomalies, suggesting that the warming trend is caused by an increase in the advective heat flux convergence related to the weakened DSW transport from the northwestern shelf.

In the WFLX experiment, the flux decrease in the DSW flux is achieved through SSS, by a change in the surface freshwater flux. The linear trend for the monthly SSS over the northwestern shelf region (Fig. 14b) indicates a decrease in SSS throughout the year, although the negative trend is somewhat large around May and November–December. Additional perturbation experiments in relation

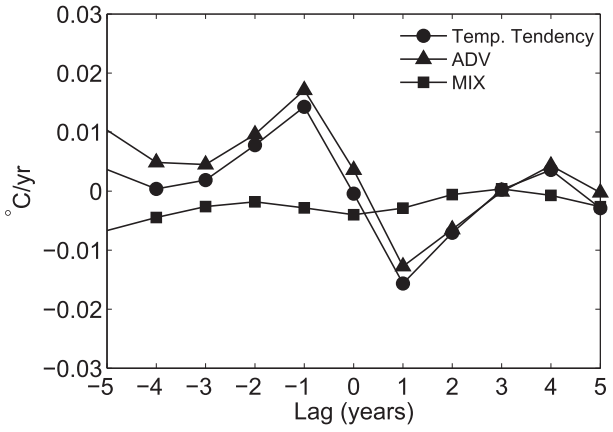

FIG. 15. As in Fig. 12, but for the subarctic frontal region in the WSTR experiment.

to precipitation (WFLX-P) and evaporation (WFLX-E) show that the SSS reduction over the northwestern shelf region is largely related to an increase in precipitation (Fig. 14b).

3) WSTR EXPERIMENT

In the Okhotsk Sea, the temperature tendency is also approximately explained by the ADV term (Fig. 12c). The regression map of the ADV term at lag −1 yr (Fig. 13c) shows that the positive regression along the western part of the Okhotsk Sea is related to the northward heat flux anomalies. Since the potential temperature has decreased in the WSTR experiment, this result suggests that the cooling trend is caused mainly by the decrease in the advective heat flux convergence related to the strengthened DSW transport from the northwestern shelf.

In the western subarctic front, the heat budget is also dominated by the ADV term (Fig. 15). The regression map of the ADV term at lag −1 yr (Fig. 16) shows that the positive regression zonally extends eastward along 45°N, which corresponds to the warming trend in the subarctic region (Fig. 10c). This positive regression is related to the northeastward anomalies of advective heat flux around 43°N, 147°–150°E. Since this region corresponds to the wind-driven gyre boundary between the subarctic and subtropical gyre, it is suggested that the warming trend along the subarctic frontal region is caused by the increase in the subtropical water transport.

Since the temperature tendency in the Sea of Okhotsk and subarctic frontal region are approximately explained mostly by the ADV term associated with the large-scale flow (Figs. 12c and 15), the relationship between the changes in the advective heat flux and large-scale ocean circulation was briefly examined using barotropic transport streamfunction (Ψ) defined as follows:

$$\Psi = \int_{y_N}^{y} U\, dy, \tag{2}$$

where U is the zonal component of vertically integrated volume transport, y_N is the northern boundary of the model domain. Thus, Ψ is nondivergent and approximately the streamfunction of geostrophic transport in the basin.

Figure 17a shows the climatology of annually averaged Ψ in the WSTR. The cyclonic circulations are dominant in the Okhotsk Sea and in the western subarctic North Pacific. In addition, the simulated water

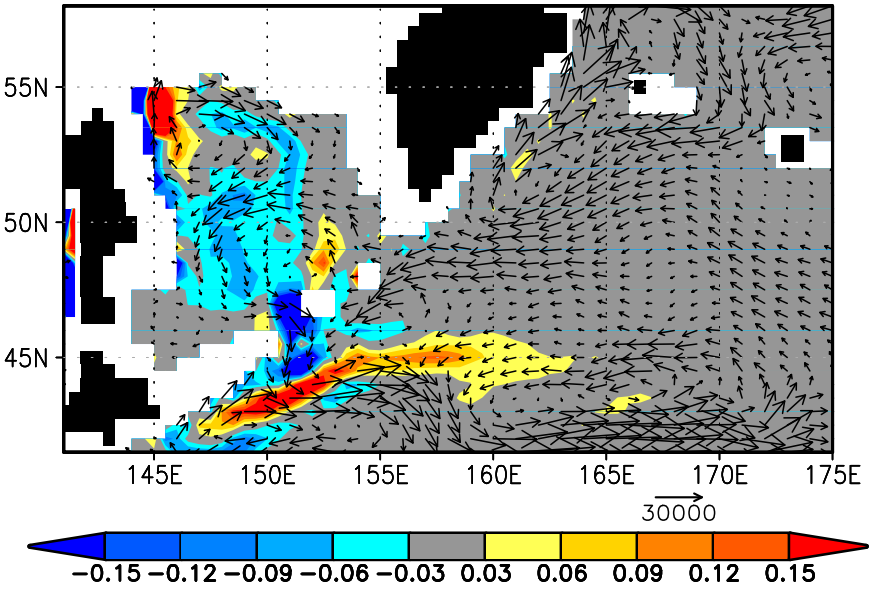

FIG. 16. As in Fig. 13, but for region B, calculated from the WSTR experiment.

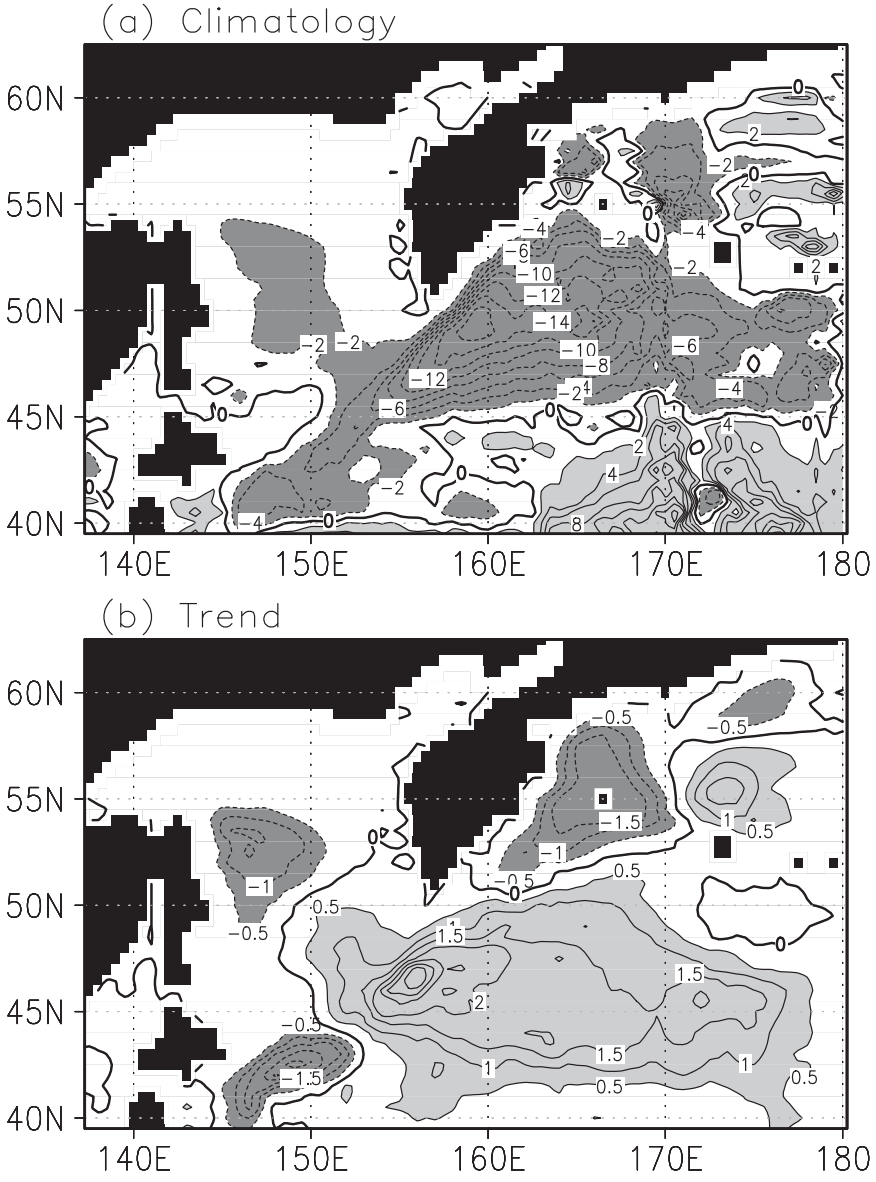

FIG. 17. (a) Climatology (Sv), and (b) linear trend [Sv $(30\,\mathrm{yr})^{-1}$] of annually averaged Ψ in the WSTR experiment. The contour interval is 2 Sv and 0.5 Sv $(30\,\mathrm{yr})^{-1}$ in (a) and (b), respectively. Negative values indicate cyclonic circulation. The light (dense) shading indicates positive (negative) values larger (less) than 2 Sv and 0.5 Sv $(30\,\mathrm{yr})^{-1}$ in (a) and (b), respectively.

exchange between the Okhotsk Sea and the North Pacific occurs through inflow from the Pacific via the Kruzenshtern Strait, and outflow from the Okhotsk Sea via the Bussol' Strait; this is in agreement with suggestions from observations (Ohshima et al. 2010).

The trend map of annually averaged Ψ reveals a strengthening of the cyclonic circulation in the Okhotsk Sea (Fig. 17b). Since the climatological potential temperature along the Sakhalin Island is relatively cold in the northern part (Fig. 2d), it is considered that the decrease in the advective heat flux convergence in the corresponding density is caused by both a strengthened southward transport anomaly and an increase in DSW density, which is related to the enhanced northward transport of the saline water from the Pacific (Matsuda et al. 2009). On the other hand, the trend of Ψ in the western subarctic gyre (Fig. 17b) indicates that the increase in the subtropical water transport is related to the northward trend around 43°N, 147°–150°E associated with the positive trend in subarctic gyre. We also looked at the northward shift of the subarctic front as this could also form a zonal pattern of

the increased potential temperature. However, the simulated front moves southward by about 0.1° latitude, which is opposite sense to the warming trend. The effect of the meridional shift on the warming trend is thus considered to be negligible.

There is a seasonal dependence on the ocean circulation changes responsible for the cooling in the Okhotsk Sea and the warming in the western subarctic North Pacific. Figure 18 shows the linear trend in the monthly mean Ψ in the Okhotsk Sea (53°N, 147°E) and the western subarctic North Pacific (47°N, 155°E). The ocean circulation in the Okhotsk Sea is strengthened with maximum peaks in early (November) and late (March) winter (Fig. 18a), and in contrast there is a large weakening of the ocean circulation in the western subarctic North Pacific in early and late winter (Fig. 18b). It is thus evident that the winter season is the key season for the cooling in the Sea of Okhotsk and warming in the subarctic frontal region simulated in WSTR experiment, and this is in agreement with the results from the HEAT and WFLX experiments.

d. Atmospheric forcing pattern related to the trend

Analysis of the perturbation experiments has shown that 1) turbulent heat flux causes warming through a decrease in sea ice production, 2) freshwater flux ($P - E$) causes warming through a decrease in SSS, and 3) wind stress causes cooling in the Okhotsk Sea and warming in the subarctic region through the wind-driven circulation change. In this section we investigate the changes in atmospheric conditions responsible for these changes (i.e., changes in surface air temperature, precipitation, and wind stress curl), and the related atmospheric circulation patterns. Since the trends revealed by the HEAT, WFLX, and WSTR experiments are large in early and late winter, we focus on the trend patterns of atmospheric conditions in March (the trend patterns in November are similar to those in March).

Figures 19a and 19b show the trend maps of surface air temperature and precipitation in late winter (March). The positive trend of surface air temperature and precipitation is seen to be significant over the Okhotsk Sea, as is consistent with the results of the HEAT-T and WFLX-P experiments. It is noted that the maximum of the positive trend in air temperature over the central part of the Okhotsk Sea is partly related to the reduction in sea ice; this is evident because the sea ice cover acts as an insulator obstructing the heat fluxes between the ocean and atmosphere (Inoue et al. 2003). The wind stress curl in March is also significantly strengthened and weakened in the Okhotsk Sea and the subarctic North Pacific, respectively (Fig. 19c). Thus, the strengthened wind stress curl over the Okhotsk Sea enhances the cyclonic circulation and results in the increase in the DSW flux. On the other hand, the weakened wind stress curl over the North Pacific suppresses the subarctic gyre and resulted in the enhancement of the northward flux of the subtropical water.

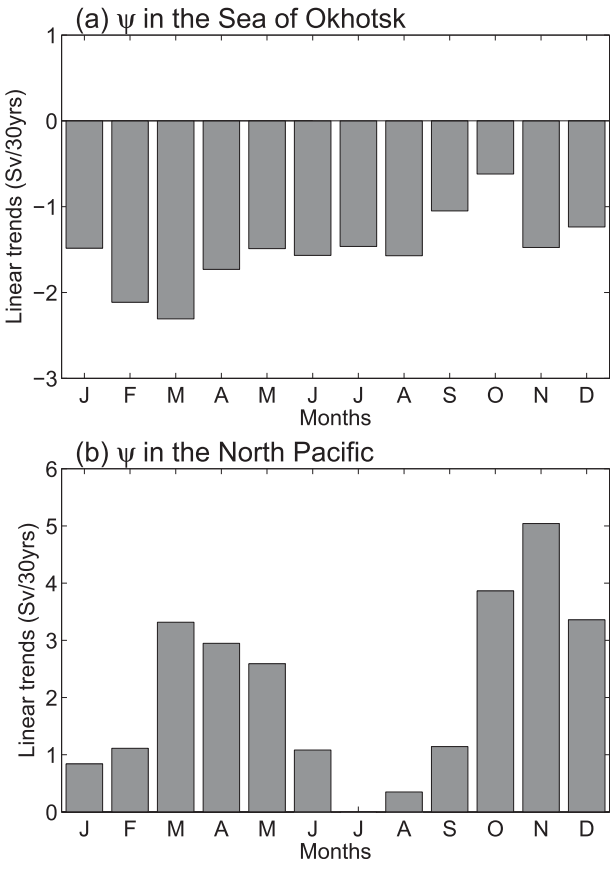

FIG. 18. Linear trends [psu $(30\,\mathrm{yr})^{-1}$] in monthly Ψ in (a) the cyclonic circulation in the Okhotsk Sea (53°N, 147°E) and (b) the western subarctic gyre (47°N, 155°E) in the WSTR experiment.

Figure 19d shows the linear trends of sea level pressure in late winter (March). Significant positive and negative trends are found over the North Pacific and far eastern Eurasia, respectively, suggesting that the trend patterns of atmospheric conditions are related to the weakened Siberian high (SH) and the Aleutian low (AL) in late winter. Similar trend patterns of the weakened AL are also found in November, although the weakening trend in SH is obscure (not shown). It is thus suggested that these trend patterns are related to a shortened period of the East Asian winter monsoon. Such atmospheric patterns are also simulated in a coupled atmosphere–ocean general circulation model simulation under the global warming scenario (Hori and Ueda 2006). It is therefore considered that the trend patterns of these atmospheric conditions, and the

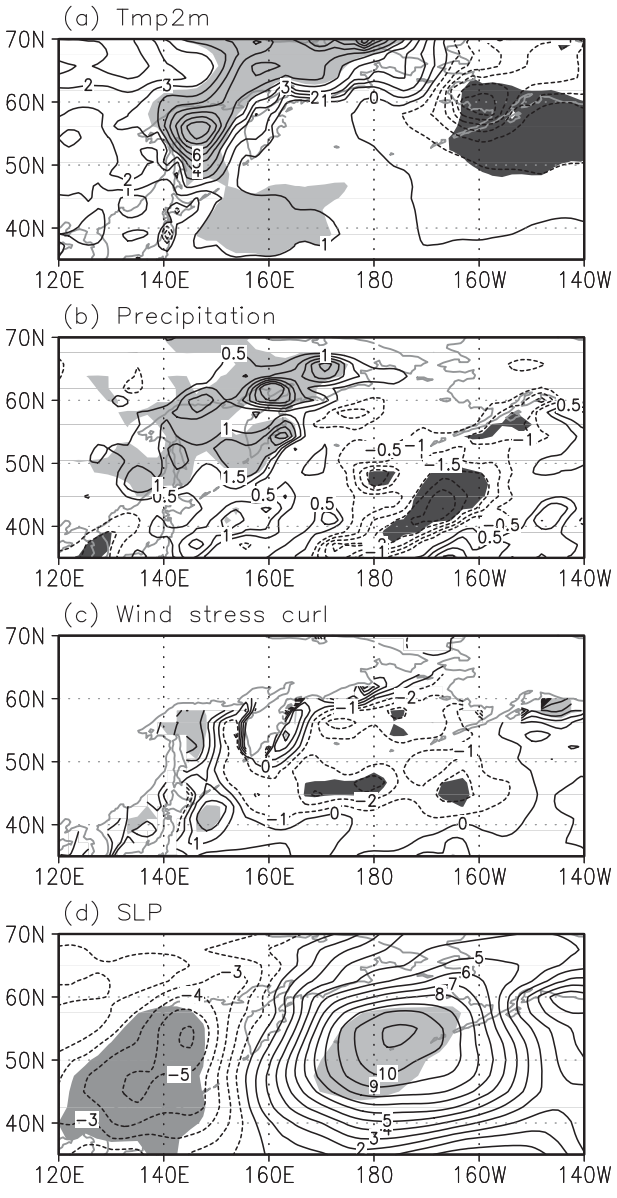

FIG. 19. Linear trends in: (a) surface air temperature [°C $(30\,\mathrm{yr})^{-1}$], (b) precipitation [mm $(30\,\mathrm{yr})^{-1}$], (c) wind stress curl [$\times 10^{-7}\,\mathrm{N\,m^{-3}}\,(30\,\mathrm{yr})^{-1}$], and (d) sea level pressure [hPa $(30\,\mathrm{yr})^{-1}$] in March, as calculated from NCEP–NCAR reanalysis data during the period 1980 to 2008. Shading indicates regions where trends are significant at the 95% confidence level, based on the *t* test.

related warming of the intermediate water, are expected to accelerate in the future.

However, the strength of the Aleutian low in spring has an interdecadal fluctuation on a 50- to 70-yr time scale, which is associated with the Pacific decadal oscillation (PDO) (Minobe 2000). Since the period of our simulation (1980–2008) corresponds to the weak phase of the Aleutian low (Bond et al. 2003), the PDO may partly contribute to the atmospheric condition trend patterns in the subarctic North Pacific, and the warming trend of the intermediate water in the Okhotsk Sea. Since it is difficult to evaluate the quantitative effects of global warming and the PDO on the warming trend by use of the present reanalysis data, such a study is considered to be future work.

5. Summary and discussion

Using an ice–ocean coupled model we evaluated the effects of interannual variability of atmospheric forcing on the multidecadal-scale warming in and around the Okhotsk Sea during 1980–2008 and explored the possible mechanisms. The hindcast experiment qualitatively simulates the observed warming of the intermediate water in and around the Okhotsk Sea. The significant warming trend is seen to be remarkable in the western part of the Okhotsk Sea and the subarctic frontal region on the isopycnal surfaces of (26.9–27.1)σ_θ. These significant warming trends are also simulated by several sensitivity experiments on the freshwater fluxes and tidal mixing parameters.

The roles of sea ice production, freshening due to freshwater flux, and wind-driven ocean circulation on the warming signal on the isopycnal surface of 27.0σ_θ were examined based on a set of model experiments with artificial perturbations in surface fluxes, by separately imposing interannual variations of turbulent heat flux (HEAT), freshwater flux (WFLX), and wind stress (WSTR), respectively. The comparison between the three perturbation experiments indicates that surface heat and freshwater fluxes contribute positively to the warming of intermediate water in the Okhotsk Sea (OSIW), whereas the wind stress contributes negatively. The warming of the OSIW can be explained by the superposition of these temperature variations.

A heat budget analysis indicates that the warming of the OSIW induced by the turbulent heat and surface freshwater fluxes is mostly explained by a decrease in DSW flux. Additional perturbation experiments on the turbulent heat flux suggest that the warming of the surface air temperature is responsible for the decrease in sea ice production, which results in a decrease in the production of DSW. This supports the previous hypothesis of Nakanowatari et al. (2007) and is consistent with the recent study by Kashiwase et al. (2014), who indicated that the negative trend of sea ice production estimated from heat flux calculations using satellite-based ice thickness and atmospheric reanalysis data is mainly explained by the warming of autumn air temperature in the northwest of the Okhotsk Sea.

The present simulation suggests that surface freshwater flux, particularly precipitation, has a substantial

impact on the warming of the OSIW through the freshening of the surface water, which then leads to a decrease in the DSW flux. Since the warming on the isopycnal surface is translated to a salination signal due to the surrounding *T*–*S* curve, this result is inconsistent with the hypothesis by Wong et al. (1999, 2001), who suggest that fresher surface water feeds to the ventilation regions such as Okhotsk Sea and their signals are advected along the formation pathway for NPIW. Thus, it is suggested that the recent freshening in NPIW is not directly related to the modified OSIW. Since the freshwater flux change in the OSIW may be overestimated in the hindcast experiment, further quantitative evaluations of the change in the freshwater flux over the polar region are needed for the precise contribution on the change in the intermediate water property.

Our numerical experiments also suggest that wind stress has a role in cooling the OSIW through an increase in the DSW. Among previous studies, Matsuda et al. (2009) suggested that the stronger wind-driven circulation in the Okhotsk Sea leads to an enhancement of the DSW flux, through both an increase in DSW density caused by the northward transport of the saline water from the Pacific and an increase in DSW transport from the shelf to the interior. Our study suggests that these processes substantially affect the water properties in the Okhotsk Sea on multidecadal time scale.

On the other hand, the change in wind-driven ocean circulation makes a substantial contribution to the warming of the western subarctic North Pacific, although the effects of advection of the warmed OSIW caused by the turbulent heat and freshwater fluxes are not negligible. The analysis of ocean heat content demonstrates that the warming trend in the western subarctic North Pacific is caused by the increase in the northward transport of the subtropical water. However, it is possible that the supply of warmed OSIW to this region has been underestimated, because the temperature and salinity are restored to the climatological value near the southern boundary in our experiment. A further examination using a global model simulation is needed to clarify the effects of the thermohaline- or wind-driven processes on the warming trend in the North Pacific.

Acknowledgments. Numerical calculations were performed using HITACHI SR16000 at the high performance computing system of Hokkaido University, and at the Center for Climate System Research at Tokyo University (under cooperative research programs); and using SGI UV1000 at the Pan-Okhotsk Information System of Hokkaido University. A number of figures were produced using the GrADS package developed by B. Doty. This work was supported by a fund from Grant-in-Aid for Scientific Research (19340131, 20221001, 22221001), Core Research for Evolution Science and Technology (CREST), Japan Science and Technology Corporation (JST), Joint Usage/Research Center for Interdisciplinary Large-scale Information Infrastructures (JHPCN), and Global COE Program ''Establishment of Center for Integrated Field Environmental Science,'' MEXT, Japan.

REFERENCES

Andreev, A. G., and G. V. Shevchenko, 2008: Interannual variability of water transport by the East Kamchatka and East Sakhalin Currents and their influence on dissolved oxygen concentration in the Sea of Okhotsk and subarctic Pacific. *Russ. Meteor. Hydrol.,* **33,** 657–664, doi:10.3103/S1068373908100075.

Argo Science Team, 2001: The global array of profiling floats. *Observing the Ocean in the 21st Century,* C. J. Koblinsky and N. R. Smith, Eds., Australian Bureau of Meteorology, 248–258.

Bond, N. A., J. E. Overland, M. Spillane, and P. Stabeno, 2003: Recent shifts in the state of the North Pacific. *Geophys. Res. Lett.,* **30,** 2183, doi:10.1029/2003GL018597.

Boyer, T. P., C. Stephens, J. I. Antonov, M. E. Conkright, R. A. Locarnini, T. D. O'Brien, and H. E. Garcia, 2002: *Salinity.* Vol. 1, *World Ocean Atlas 2001,* NOAA Atlas NESDIS 50, 176 pp.

Conkright, M. E., and Coauthors, 2002: *Introduction.* Vol. 1, *World Ocean Database 2001,* NOAA Atlas NESDIS 42, 167 pp.

Cox, M. D., 1987: Isopycnal diffusion in a *z*-coordinate ocean model. *Ocean Modell.,* **74,** 1–5.

Dai, A., and K. E. Trenberth, 2002: Estimates of freshwater discharge from continents: Latitudinal and seasonal variations. *J. Hydrometeor.,* **3,** 660–687, doi:10.1175/1525-7541(2002)003<0660:EOFDFC>2.0.CO;2.

Ducet, N., P. Y. Le Traon, and G. Reverdin, 2000: Global high-resolution mapping of ocean circulation from TOPEX/Poseidon and ERS-1 and -2. *J. Geophys. Res.,* **105,** 19 477–19 498, doi:10.1029/2000JC900063.

Durack, P. J., and S. E. Wijffels, 2010: Fifty-year trends in global ocean salinities and their relationship to broad-scale warming. *J. Climate,* **23,** 4342–4362, doi:10.1175/2010JCLI3377.1.

Fujisaki, A., H. Mitsudera, and H. Yamaguchi, 2011: Dense shelf water formation process in the Sea of Okhotsk based on an ice-ocean coupled model. *J. Geophys. Res.,* **116,** C03005, doi:10.1029/2009JC006007.

Fukamachi, Y., G. Mizuta, K. I. Ohshima, L. D. Talley, S. C. Riser, and M. Wakatsuchi, 2004: Transport and modification processes of dense shelf water revealed by long-term moorings off Sakhalin in the Sea of Okhotsk. *J. Geophys. Res.,* **109,** C09S10, doi:10.1029/2003JC001906.

Gent, P. R., and J. C. McWilliams, 1990: Isopycnal mixing in ocean circulation models. *J. Phys. Oceanogr.,* **20,** 150–155, doi:10.1175/1520-0485(1990)020<0150:IMIOCM>2.0.CO;2.

Gladyshev, S., S. Martin, S. Riser, and A. Figurkin, 2000: Dense water production on the northern Okhotsk shelves: Comparison of ship-based spring–summer observations for 1996 and 1997 with satellite observations. *J. Geophys. Res.,* **105** (C11), 26 281–26 299, doi:10.1029/1999JC000067.

Hansell, D. A., C. A. Carlson, and Y. Suzuki, 2002: Dissolved organic carbon export with North Pacific Intermediate Water formation. *Global Biogeochem. Cycles,* **16,** 1007, doi:10.1029/2000GB001361.

Hasumi, H., 2006: CCSR Ocean Component Model (COCO) version 4.0. Tech. Rep. 25, Center for Climate Systems Research, University of Tokyo, 103 pp.

Hill, K. L., A. J. Weaver, H. J. Freeland, and A. Bychkov, 2003: Evidence of change in the Sea of Okhotsk: Implications for the North Pacific. *Atmos.–Ocean,* **41,** 49–63, doi:10.3137/ao.410104.

Hori, M. E., and H. Ueda, 2006: Impact of global warming on the East Asian winter monsoon as revealed by nine coupled atmosphere–ocean GCMs. *Geophys. Res. Lett.,* **33,** L03713, doi:10.1029/2005GL024961.

Hosoda, S., T. Sugo, N. Shikama, and K. Mizuno, 2009: Global surface layer salinity change detected by Argo and its implication for hydrological cycle intensification. *J. Oceanogr.,* **65,** 579–586, doi:10.1007/s10872-009-0049-1.

Hunke, E., and J. K. Dukowicz, 1997: An elastic-viscous-plastic model for sea ice dynamics. *J. Phys. Oceanogr.,* **27,** 1849–1867, doi:10.1175/1520-0485(1997)027<1849:AEVPMF>2.0.CO;2.

Inoue, J., J. Ono, Y. Tachibana, M. Honda, K. Iwamoto, Y. Fujiyoshi, and K. Takeuchi, 2003: Characteristics of heat transfer over the ice-covered Sea of Okhotsk during cold air outbreaks. *J. Meteor. Soc. Japan,* **81,** 1057–1067, doi:10.2151/jmsj.81.1057.

Isoguchi, O., H. Kawamura, and E. Oka, 2006: Quasi-stationary jets transporting surface warm waters across the transition zone between the subtropical and the subarctic gyres in the North Pacific. *J. Geophys. Res.,* **111,** C10003, doi:10.1029/2005JC003402.

Ito, S., K. Uehara, T. Miyaho, H. Miyake, I. Yasuda, T. Watanabe, and Y. Shimizu, 2004: Characteristics of SSH anomaly based on TOPEX/Poseidon altimetry and in situ measured velocity and transport of Oyashio on OICE. *J. Oceanogr.,* **60,** 425–437, doi:10.1023/B:JOCE.0000038059.54334.6b.

Itoh, M., 2007: Warming of intermediate water in the Sea of Okhotsk since the 1950s. *J. Oceanogr.,* **63,** 637–641, doi:10.1007/s10872-007-0056-z.

——, K. I. Ohshima, and M. Wakatsuchi, 2003: Distribution and formation of Okhotsk Sea Intermediate Water: An analysis of isopycnal climatological data. *J. Geophys. Res.,* **108,** 3258, doi:10.1029/2002JC001590.

Itoh, S., and I. Yasuda, 2010: Water mass structure of warm and cold anticyclonic eddies in the western boundary region of the subarctic North Pacific. *J. Phys. Oceanogr.,* **40,** 2624–2642, doi:10.1175/2010JPO4475.1.

Japan Oceanographic Data Center, 2003: J-DOSS: JODC Data On-line Service System. [Available online at http://www.jodc.go.jp/service.htm.]

Kalnay, E. M., and Coauthors, 1996: The NCEP/NCAR 40-Year Reanalysis Project. *Bull. Amer. Meteor. Soc.,* **77,** 437–471, doi:10.1175/1520-0477(1996)077<0437:TNYRP>2.0.CO;2.

Kaplan, D., and L. Glass, 1995: *Understanding Nonlinear Dynamics.* Springer-Verlag, 420 pp.

Kara, A. B., P. A. Rochford, and H. E. Hurlburt, 2000: Efficient and accurate bulk parameterizations of air–sea fluxes for use in general circulation models. *J. Atmos. Oceanic Technol.,* **17,** 1421–1438, doi:10.1175/1520-0426(2000)017<1421:EAABPO>2.0.CO;2.

Kashiwase, H., K. I. Ohshima, and S. Nihashi, 2014: Long-term variation in sea ice production and its relation to the intermediate water in the Okhotsk Sea. *Prog. Oceanogr.,* **126,** 21–32, doi:10.1016/j.pocean.2014.05.004.

Katsumata, K., and I. Yasuda, 2010: Estimates of non-tidal exchange transport between the Sea of Okhotsk and the North Pacific. *J. Oceanogr.,* **66,** 489–504, doi:10.1007/s10872-010-0041-9.

Kawaguchi, Y., S. Nihashi, H. Mitsudera, and K. I. Ohshima, 2010: Formation mechanism of huge coastal polynyas and its application to Okhotsk northwestern polynya. *J. Phys. Oceanogr.,* **40,** 2451–2465, doi:10.1175/2010JPO4304.1.

Kawasaki, Y., and T. Kono, 1994: Distribution and transport of subarctic waters around the middle of Kuril Islands (in Japanese with English abstract and figure captions). *Umi Sora,* **70,** 71–84.

Kitani, K., 1973: An oceanographic study of the Okhotsk Sea: Particularly in regard to cold waters. *Bull. Far Sea Fish. Res. Lab.,* **9,** 45–77.

Kono, T., and Y. Kawasaki, 1997: Results of CTD and mooring observations southeast of Hokkaido. 1. Annual velocity and transport variations in the Oyashio. *Bull. Hokkaido Natl. Fish. Res. Inst.,* **61,** 65–81.

Leonard, B. P., 1979: A stable and accurate convective modeling procedure based on quadratic upstream interpolation. *Comput. Methods Appl. Mech. Eng.,* **19,** 59–98, doi:10.1016/0045-7825(79)90034-3.

——, M. K. MacVean, and A. P. Lock, 1995: The flux integral method for multidimensional convection and diffusion. *Appl. Math. Modell.,* **19,** 333–342, doi:10.1016/0307-904X(95)00017-E.

Levitus, S., and T. Boyer, 1994: *Temperature.* Vol. 4, *World Ocean Atlas 1994,* NOAA Atlas NESDIS 4, 117 pp.

Martin, S., R. Drucker, and K. Yamashita, 1998: The production of ice and dense shelf water in the Okhotsk Sea polynyas. *J. Geophys. Res.,* **103** (C12), 27 771–27 782, doi:10.1029/98JC02242.

Masumoto, Y., and Coauthors, 2004: A fifty-year eddy-resolving simulation for the World Ocean—Preliminary outcomes of OFES (OGCM for the Earth Simulator). *J. Earth Simul.,* **1,** 35–56.

Matsuda, J., H. Mitsudera, T. Nakamura, K. Uchimoto, T. Nakanowatari, and N. Ebuchi, 2009: Wind and buoyancy driven intermediate-layer overturning in the Sea of Okhotsk. *Deep-Sea Res. I,* **56,** 1401–1418, doi:10.1016/j.dsr.2009.04.014.

Minobe, S., 2000: Spatio-temporal structure of the pentadecadal variability over the North Pacific. *Prog. Oceanogr.,* **47,** 381–408, doi:10.1016/S0079-6611(00)00042-2.

——, and T. Nakanowatari, 2002: Global structure of bidecadal precipitation variability in boreal winter. *Geophys. Res. Lett.,* **29,** 1396, doi:10.1029/2001GL014447.

Mizuta, G., Y. Fukamachi, K. I. Ohshima, and M. Wakatsuchi, 2003: Structure and seasonal variability of the East Sakhalin Current. *J. Phys. Oceanogr.,* **33,** 2430–2445, doi:10.1175/1520-0485(2003)033<2430:SASVOT>2.0.CO;2.

Nakamura, T., and T. Awaji, 2004: Tidally induced diapycnal mixing in the Kuril Straits and its role in water transformation and transport: A three-dimensional non-hydrostatic model experiment. *J. Geophys. Res.,* **109,** C09S07, doi:10.1029/2003JC001850.

——, ——, T. Hatayama, K. Akitomo, and T. Takizawa, 2000a: Tidal exchange through the Kuril Straits. *J. Phys. Oceanogr.,* **30,** 1622–1644, doi:10.1175/1520-0485(2000)030<1622:TETTKS>2.0.CO;2.

——, ——, ——, ——, ——, T. Kono, Y. Kawasaki, and M. Fukasawa, 2000b: The generation of large-amplitude unsteady lee waves by subinertial K_1 tidal flow: A possible vertical mixing mechanism in the Kuril Straits. *J. Phys. Oceanogr.,* **30,** 1601–1621, doi:10.1175/1520-0485(2000)030<1601:TGOLAU>2.0.CO;2.

——, T. Toyoda, Y. Ishikawa, and T. Awaji, 2006: Enhanced ventilation in the Okhotsk Sea through tidal mixing at the Kuril Straits. *Deep-Sea Res. I,* **53,** 425–448, doi:10.1016/j.dsr.2005.12.006.

——, Y. Kawasaki, T. Kono, and T. Awaji, 2010: Large-amplitude internal waves observed in the Kruzenshtern Strait of the

Kuril Island Chain and possible water transport and mixing. *Cont. Shelf Res.,* **30,** 598–607, doi:10.1016/j.csr.2009.07.010.

Nakanowatari, T., K. I. Ohshima, and M. Wakatsuchi, 2007: Warming and oxygen decrease of intermediate water in the northwestern North Pacific, originating from the Sea of Okhotsk, 1995–2004. *Geophys. Res. Lett.,* **34,** L04602, doi:10.1029/2006GL028243.

——, H. Mitsudera, T. Motoi, K. I. Ohshima, and I. Ishikawa, 2010: 50-yr scale cooling in North Pacific Intermediate Water simulated by eddy resolving ice-ocean coupled model (in Japanese with English abstract and figure captions). *Umi Sora,* **85,** 141–150.

Nakatsuka, T., M. Toda, K. Kawamura, and M. Wakatsuchi, 2004: Dissolved and particulate organic carbon in the Sea of Okhotsk: Transport from continental shelf to ocean interior. *J. Geophys. Res.,* **109,** C09S14, doi:10.1029/2003JC001909.

Nihashi, S., K. I. Ohshima, T. Tamura, Y. Fukamachi, and S. Saitoh, 2009: Thickness and production of sea ice in the Okhotsk Sea coastal polynyas from AMSR-E. *J. Geophys. Res.,* **114,** C10025, doi:10.1029/2008JC005222.

——, ——, and N. Kimura, 2012: Creation of a heat and salt flux dataset associated with sea ice production and melting in the Sea of Okhotsk. *J. Climate,* **25,** 2261–2278, doi:10.1175/JCLI-D-11-00022.1.

Nishioka, J., and Coauthors, 2007: Iron supply to the western subarctic Pacific: Importance of iron export from the Sea of Okhotsk. *J. Geophys. Res.,* **112,** C10012, doi:10.1029/2006JC004055.

Noh, Y., and H. J. Kim, 1999: Simulations of temperature and turbulence structure of the oceanic boundary layer with the improved near-surface process. *J. Geophys. Res.,* **104,** 15 621–15 634, doi:10.1029/1999JC900068.

Nonaka, M., H. Nakamura, Y. Tanimoto, T. Kagimoto, and H. Sasaki, 2008: Interannual-to-decadal variability in the Oyashio and its influence on temperature in the subarctic frontal zone: An eddy-resolving OGCM simulation. *J. Climate,* **21,** 6283–6303, doi:10.1175/2008JCLI2294.1.

Ohshima, K. I., T. Watanabe, and S. Nihashi, 2003: Surface heat budget of the Sea of Okhotsk during 1987–2001 and the role of sea ice on it. *J. Meteor. Soc. Japan,* **81,** 653–677, doi:10.2151/jmsj.81.653.

——, D. Simizu, M. Itoh, G. Mizuta, Y. Fukamachi, S. C. Riser, and M. Wakatsuchi, 2004: Sverdrup balance and the cyclonic gyre in the Sea of Okhotsk. *J. Phys. Oceanogr.,* **34,** 513–525, doi:10.1175/1520-0485(2004)034<0513:SBATCG>2.0.CO;2.

——, T. Nakanowatari, S. C. Riser, and M. Wakatsuchi, 2010: Seasonal variation in the in- and outflow of the Okhotsk Sea with the North Pacific. *Deep-Sea Res. II,* **57,** 1247–1256, doi:10.1016/j.dsr2.2009.12.012.

——, ——, ——, Y. N. Volkov, and M. Wakatsuchi, 2014: Freshening and dense shelf water reduction in the Okhotsk Sea, linked with sea ice decline. *Prog. Oceanogr.,* **126,** 71–79, doi:10.1016/j.pocean.2014.04.020.

Osafune, S., and I. Yasuda, 2006: Bidecadal variability in the intermediate waters of the northwestern subarctic Pacific and the Okhotsk Sea in relation to 18.6-year period nodal tidal cycle. *J. Geophys. Res.,* **111,** C05007, doi:10.1029/2005JC003277.

Qiu, B., 2002: Large-scale variability in the midlatitude subtropical and subpolar North Pacific Ocean: Observations and causes. *J. Phys. Oceanogr.,* **32,** 353–375, doi:10.1175/1520-0485(2002)032<0353:LSVITM>2.0.CO;2.

Rayner, N. A., D. E. Parker, E. B. Horton, C. K. Folland, L. V. Alexander, and D. P. Rowell, 2003: Global analyses of sea surface temperature, sea ice, and night marine air temperature since the late nineteenth century. *J. Geophys. Res.,* **108** (D14), 4407, doi:10.1029/2002JD002670.

Sasajima, Y., H. Hasumi, and T. Nakamura, 2010: A sensitivity study of the dense shelf water formation in the Okhotsk Sea. *J. Geophys. Res.,* **115,** C11007, doi:10.1029/2009JC005697.

Semtner, A. J., Jr., 1976: A model for the thermodynamic growth of sea ice in numerical investigations of climate. *J. Phys. Oceanogr.,* **6,** 379–389, doi:10.1175/1520-0485(1976)006<0379:AMFTTG>2.0.CO;2.

Serreze, M. C., and Coauthors, 2000: Observational evidence of recent change in the northern high-latitude environment. *Climatic Change,* **46,** 159–207, doi:10.1023/A:1005504031923.

——, A. P. Barnett, and F. Lo, 2005: Northern high-latitude precipitation as depicted by atmospheric reanalyses and satellite retrievals. *Mon. Wea. Rev.,* **133,** 3407–3430, doi:10.1175/MWR3047.1.

Shcherbina, A. Y., L. D. Talley, and D. L. Rudnick, 2003: Direct observations of North Pacific ventilation: Brine rejection in the Okhotsk Sea. *Science,* **302,** 1952–1955, doi:10.1126/science.1088692.

Smagorinsky, J., 1963: General circulation experiments with the primitive equations. *Mon. Wea. Rev.,* **91,** 99–164, doi:10.1175/1520-0493(1963)091<0099:GCEWTP>2.3.CO;2.

Stephens, C., J. I. Antonov, T. P. Boyer, M. E. Conkright, R. A. Locarnini, T. D. O'Brien, and H. E. Garcia, 2002: *Temperature.* Vol. 1, *World Ocean Atlas 2001,* NOAA Atlas NESDIS 49, 176 pp.

Tachibana, Y., K. Oshima, and M. Ogi, 2008: Seasonal and interannual variations of Amur River discharge and their relationships to large-scale atmospheric patterns and moisture fluxes. *J. Geophys. Res.,* **113,** D16102, doi:10.1029/2007JD009555.

Talley, L. D., 1991: An Okhotsk Sea water anomaly: Implications for ventilation in the North Pacific. *Deep Sea Res.,* **38A** (suppl.), S171–S190, doi:10.1016/S0198-0149(12)80009-4.

Tanaka, Y., T. Hibiya, Y. Niwa, and N. Iwamae, 2010: Numerical study of K_1 internal tides in the Kuril Straits. *J. Geophys. Res.,* **115,** C09016, doi:10.1029/2009JC005903.

Uchimoto, K., T. Nakamura, J. Nishioka, H. Mitsudera, M. Yamamoto-Kawai, K. Misumi, and D. Tsumune, 2011: Simulations of chlorofluorocarbons in and around the Sea of Okhotsk: Effects of tidal mixing and brine rejection on the ventilation. *J. Geophys. Res.,* **116,** C02034, doi:10.1029/2010JC006487.

——, ——, ——, ——, K. Misumi, D. Tsumune, and M. Wakatsuchi, 2014: Simulation of high concentration of iron in dense shelf water in the Okhotsk Sea. *Prog. Oceanogr.,* **126,** 194–210, doi:10.1016/j.pocean.2014.04.018.

Uehara, H., A. A. Kruts, Y. N. Volkov, T. Nakamura, T. Ono, and H. Mitsudera, 2012: A new climatology of the Okhotsk Sea derived from the FERHRI database. *J. Oceanogr.,* **68,** 869–886, doi:10.1007/s10872-012-0147-3.

——, ——, H. Mitsudera, T. Nakamura, Y. N. Volkov, and M. Wakatsuchi, 2014: Remotely propagating salinity anomaly varies the source of the North Pacific ventilation. *Prog. Oceanogr.,* **126,** 80–97, doi:10.1016/j.pocean.2014.04.016.

Warner, M. J., J. L. Bullister, D. P. Wisegraver, R. H. Gammon, and R. F. Weiss, 1996: Basinwide distributions of chlorofluorocarbons CFC-11 and CFC-12 in the North Pacific: 1985–1989. *J. Geophys. Res.,* **101** (C9), 20 525–20 542, doi:10.1029/96JC01849.

Watanabe, T., and M. Wakatsuchi, 1998: Formation of 26.8–26.9 σ_θ water in the Kuril Basin of the Sea of Okhotsk as a possible origin of North Pacific Intermediate Water. *J. Geophys. Res.,* **103,** 2849–2865, doi:10.1029/97JC02914.

Wong, A. P. S., N. L. Bindoff, and J. A. Church, 1999: Large-scale freshening of intermediate waters in the Pacific and Indian Oceans. *Nature,* **400,** 440–443, doi:10.1038/22733.

——, ——, and ——, 2001: Freshwater and heat changes in the North and South Pacific Oceans between the 1960s and 1985–94. *J. Climate,* **14,** 1613–1633, doi:10.1175/1520-0442(2001)014<1613:FAHCIT>2.0.CO;2.

Wong, C. S., R. J. Matear, H. J. Freeland, F. A. Whitney, and A. S. Bychkov, 1998: WOCE line P1W in the Sea of Okhotsk: 2. CFCs and the formation rate of intermediate water. *J. Geophys. Res.,* **103,** 15 625–15 642, doi:10.1029/98JC01008.

Xie, P., and P. A. Arkin, 1997: Global precipitation: A 17-year monthly analysis based on gauge observations, satellite estimates, and numerical model outputs. *Bull. Amer. Meteor. Soc.,* **78,** 2539–2558, doi:10.1175/1520-0477(1997)078<2539:GPAYMA>2.0.CO;2.

Yamamoto-Kawai, M., S. Watanabe, S. Tsunogai, and M. Wakatsuchi, 2004: Chlorofluorocarbons in the Sea of Okhotsk: Ventilation of the intermediate water. *J. Geophys. Res.,* **109,** C09S11, doi:10.1029/2003JC001919.

Yasuda, I., 1997: The origin of the North Pacific intermediate water. *J. Geophys. Res.,* **102,** 893–910, doi:10.1029/96JC02938.

Yu, L., and R. A. Weller, 2007: Objectively analyzed air–sea heat fluxes for the global ice-free oceans (1981–2005). *Bull. Amer. Meteor. Soc.,* **88,** 527–539, doi:10.1175/BAMS-88-4-527.